The Pennsylvania State University
The Graduate School

THE PERFORMANCE OF A COMPETITION SAILPLANE WITH VARIABLE-TOE WINGLETS

A Thesis in
Aerospace Engineering
by
Philip M. Chidekel

Submitted in Partial Fulfillment
of the Requirements
for the Degree of

Master of Science

May 2024

The thesis of Philip M. Chidekel was reviewed and approved by the following:

Mark D. Maughmer
Professor of Aerospace Engineering
Thesis Advisor

James G. Coder
Professor of Aerospace Engineering

Sven Schmitz
Professor of Aerospace Engineering

Amy Pritchett
Professor of Aerospace Engineering
Department Head

Abstract

The aerodynamic design of variable-toe winglets for a 15-meter-class competition sailplane has been completed using well-validated design tools. The sailplane performance is maximized at every flight condition in both cruise and climb by properly scheduling the winglet toe angle and flap setting. These variable-toe winglets enable the sailplane to access benefits that fixed-geometry winglets compromise. It is shown that variable-toe winglets substantially improve the weak-weather cross-country performance, allowing the variable-toe sailplane to climb in weaker thermals than the unmodified sailplane can use. These gains are compelling when contextualized with contest results and other modern sailplane modifications like retractable tailwheels. Concepts for control systems, structural requirements, and certification are discussed. Finally, a preliminary investigation of flapped winglets is conducted, and it is shown that the gains produced could be even more substantial than those of variable-toe winglets, particularly in cruise.

Table of Contents

List of Figures

List of Tables

List of Symbols

AR	Aspect Ratio
b	Wing Span
C_D	Aircraft Drag Coefficient
C_{D_i}	Induced Drag Coefficient
$C_{D_{profile}}$	Wing Profile-Drag Coefficient
c_d	Profile-Drag Coefficient
$c_{d_{pressure}}$	Sectional Pressure Drag Coefficient
$c_{d_{friction}}$	Sectional Skin-Friction Drag Coefficient
C_L	Aircraft Lift Coefficient
$C_{L_{tail}}$	Tail Lift Coefficient
C_{L_w}	Wing Lift Coefficient
c_l	Sectional Lift Coefficient
$C_{M_{acw}}$	Wing Pitching Moment Coefficient about the Aerodynamic Center
$C_{M_{cg}}$	Aircraft Pitching Moment Coefficient about the Center of Gravity
$C_{M_{fuse}}$	Fuselage Pitching Moment Coefficient
c	Reference Chord (m)
$\bar{\bar{c}}$	Mean Aerodynamic Chord (m)
CG	Aircraft Center of Gravity
D	Drag (N)
d	Distance (m)

e	Span Efficiency Factor
g	Gravitational Acceleration (m/s^2)
h	Height (m)
L	Lift (N)
l_{tail}	Tail Boom Length
m	Aircraft Mass (kg)
R	Turn Radius (m)
Re	Reynolds Number
S	Wing Area (m^2)
S_{tail}	Horizontal Tail Area (m^2)
t	Time (s)
V	Velocity (m/s)
V_{acc}	Average Cross-Country Speed (m/s)
V_{climb}	Climb Rate (m/s)
V_{cruise}	Cruise Speed (m/s)
V_{sink}	Sink Rate (m/s)
x_{ac_w}	Wing Aerodynamic Center Location
x_{cg}	Center of Gravity Location
α	Angle of Attack (degrees)
γ	Flight Path Angle (degrees)
μ	Dynamic Viscosity (kg/m/s)
ρ	Density (kg/m^3)
ϕ	Bank Angle (degrees)

Acknowledgments

Dr. Maughmer is foremost among those who I would like to offer my heartfelt thanks. He has been an unconventional thesis advisor in some ways–most of my aerodynamic understanding comes from conversations we've had on the porch of Ridge Soaring Gliderport or the Cafe 210 patio. I have deeply valued his friendship and mentorship over the years, and he has given me the most valuable technical gift: how to truly look at airplanes.

I have met lifelong friends in State College, and our shared adventures have enriched my life and made this place home. My colleagues in 144 Hammond have provided support, comic relief, and a wonderful environment in which we've learned challenging technical concepts together.

Finally, I would like to thank my family and my partner Fiona, who reliably and lovingly support me and my passion for aviation.

Chapter 1 Introduction

1.1 Motivation

Improving the performance of modern sailplanes is a challenging task. As shown in Table 1.1, it has taken over 40 years of effort in aerodynamics, materials, and computational methods to improve the maximum L/D of a 15-meter competition sailplane by 7.5 points. Sailplane design has reached a point of wonderful, yet frustrating maturity: modern gliders are so precisely optimized that new, meaningful improvements are increasingly difficult to achieve. Manufacturers are now experimenting with retractable tailwheels, canopy fitment, and wing root fillets to achieve even minuscule reductions in drag. Sailplane designers must look beyond the conventional to further the sport of soaring.

Of the tried-and-true performance enhancements incorporated by sailplane designers, winglets have been widely implemented for reliable and inexpensive gains in cross-country performance since the early 1990s. The design tools and understanding of the winglet design space have improved since their introduction, but modern winglets are much like the winglets designed 20 years ago: compromised for modest improvements in weak-weather climb performance and cross-country speed. Despite this, there are untried methods for winglets to meaningfully improve sailplane performance, even on modern, highly-optimized designs.

Winglet design most basically involves balancing two competing goals. The designer must reduce low-speed induced drag without increasing high-speed profile drag. This is challenging because a winglet optimized solely to increase climb performance would be dissimilar to a wingtip designed purely for efficient cruise. Therefore, the best winglet is one that compromises most gracefully between these disparate missions within the sailplane flight envelope. Although this design process improves performance despite the

Sailplane	Year Introduced	Maximum $\frac{L}{D}$
H 301 Libelle	1964	40.5
LS 3	1976	41
ASW 20	1977	41.5
Ventus B	1980	42
LS 6	1983	42
DG 600	1987	42
Ventus 2a	1994	44.5
ASW 27	1995	45.6
ASG-29-15	2006	48

Table 1.1. Improvements in 15-meter sailplane maximum L/D since the introduction of the H-301 Libelle in 1964 [3].

inherent compromises, the maximum benefits of the winglet are never realized. Therefore, the most desirable winglet could adapt in-flight from climb geometry to cruise geometry for the climb benefits of a winglet to be fully achieved while maintaining or slightly improving cruise performance. The work of this thesis is to design a sailplane winglet that accomplishes this task, and to meaningfully advance the sport of soaring through sound technical means.

1.2 Sailplanes and the Sport of Soaring

Sailplanes are some of the most elegant flight vehicles in existence. Since they are engineless, they depend entirely on diverse natural mechanisms of atmospheric lift to remain airborne. On sunny days, sailplane pilots seek thermals, which are rising columns of air generated by uneven heating of the ground. In mountainous areas, sailplanes can remain aloft using lift created as air rises over terrain and gravity waves initiated by topography or wind shear. The sport of soaring is more than simply staying airborne using these lift sources. Rather, sailplane pilots use combinations of these natural mechanisms to fly distances. These cross-country flights are composed of climbing segments to gain altitude and cruising legs to find the next lift source along the intended course of flight. Skilled pilots can traverse massive distances in this manner. Soaring flights of over 1000 km are increasingly common, and the current world distance record is held by Klaus Ohlmann, who flew a Schempp-Hirth Nimbus 4 over 3000 km in the wave produced by the Andes Mountains [7]. Gliding competitions–in which a course is fixed and pilots race for the highest average speed–are other pathways to achievement within the sport of soaring. In this manner, soaring is a challenging and engaging activity that allows sailplane pilots to interact with the natural world in a unique and compelling way. Likewise, sailplane design is equally challenging and rewarding.

At its core, the sport of soaring requires a pilot to make optimum decisions about how to manage airspeed and altitude throughout a flight. Similarly, the art of sailplane design entails presenting the pilot with a vehicle that most efficiently expends airspeed and altitude. Thus, a sailplane must extract the most energy possible from the atmosphere when climbing in lift and waste the least possible when cruising between lift sources. It therefore becomes necessary to optimize the performance of a sailplane both in high-speed cruise and in low-speed climb, presenting a formidable challenge. These are competing ends of the sailplane speed range, and improving an aircraft across its entire flight envelope is substantially more difficult than maximizing its performance for a single case. This task requires ingenuity, compromise, and innovation, and is at the center of the writing that follows.

1.3 Brief History of Wingtip Devices

Installing wingtip endplates to modify aerodynamics has been considered since at least 1897, when English polymath and engineer Frederick Lanchester included them in his patent "Improvements in and relating to Aerial Machines" [8]. Lanchester hypothesized that the wingtips of his proposed aircraft could be capped by “planes” that “minimise the lateral dissipation of the [aircraft’s] supporting wave.” Lanchester’s idea was further supported by American aircraft designer Vincent Burnelli in 1929, who also applied for a patent that included wingtip-mounted “vertical fins” which could “prevent endwise loss of pressure” [9].

Both Lanchester and Burnelli seemed to intuitively grasp that the pressure gradients at a wingtip could introduce undesirable effects. In 1937, W. Mangler confirmed these suspicions mathematically when he wrote an NACA technical memorandum describing the lift distribution on wings with endplates “for the case of minimum induced drag” [10].

Although it is logical that endplates could reduce induced drag by inhibiting spanwise flow, the added viscous drag from the increased wetted area of these wingtip plates remained an unsolved problem. In 1965, Sighard Hoerner proposed that endplates would have at least the drag of an equivalently sized set of wing tip extensions; thus, the practical applications of these designs seem limited to cases “where the plates can also be utilized for stabilizing or control purposes” [11].

The leap from endplate to winglet was completed in the 1970s by prolific NASA researcher Richard Whitcomb, who designed wingtip devices that were wind-tunnel tested and eventually flight tested on the Boeing KC-135 [12]. Whitcomb's winglets were more sophisticated than simple endplates; he tailored the airfoils, twist, and taper to achieve a lifting surface that produced reductions in drag at higher lift coefficients. His design took advantage of the induced velocities produced by the winglets to alter the flowfield of the main wing, thereby reducing spanwise flow. Whitcomb also compared the additional root bending moment applied by his wingtip devices to a simple wing extension, and concluded from both drag reduction and structural perspectives that winglets were superior to tip extensions.

Whitcomb's work helped solidify interest for installing wingtip devices on large transport aircraft. For these applications, a variety of potential options exist that have similar net improvements to overall performance [13]. These devices include winglets, tip extensions, raked wingtips, split winglets, and so on. The designer must assess the aerodynamic benefits of each option with factors such as the weight of the additional structure necessary to support the modification, the baseline lift distribution of the unmodified wing, the overall operating requirements of the aircraft, and cost. For example, the Federal Aviation Administration issued a Supplemental Type Certificate to Aviation Partners Boeing in 2000 that permits the installation of winglets onto the Boeing 737-700, 737-800, and 737-900 [14]. It is estimated from flight-test measurements that these winglets reduce the aircraft total drag in cruise by 3.2%; however, each pair of winglet assemblies weighs 300 pounds, and an additional 100 pounds of reinforcement must be added to the existing wing structure [13].

1.4 Winglet Usage on Sailplanes

The French National team flew gliders with winglets in the 1981 World Championships in Paderborn, Germany, and following the competition, Akaflieg Braunschweig designed, built, and flight tested a set of 1-meter-tall winglets for a Schleicher ASW-19. The results were once again mixed. The maximum L/D of the tested sailplane improved by 1.6 and its maximum lift coefficient increased by 0.03 with winglets; however, once the aircraft flew faster than a lift coefficient of 0.5, its performance degraded below that of the unmodified ASW-19 [15]. It was concluded that "it is only reasonable to use winglets on a glider with a limited span. A 17-m aircraft, which probably would be easier to manufacture, is far superior to a 15-m aircraft with winglets" [15]. Trials by others with different sailplanes and novel design philosophies yielded similar conclusions.

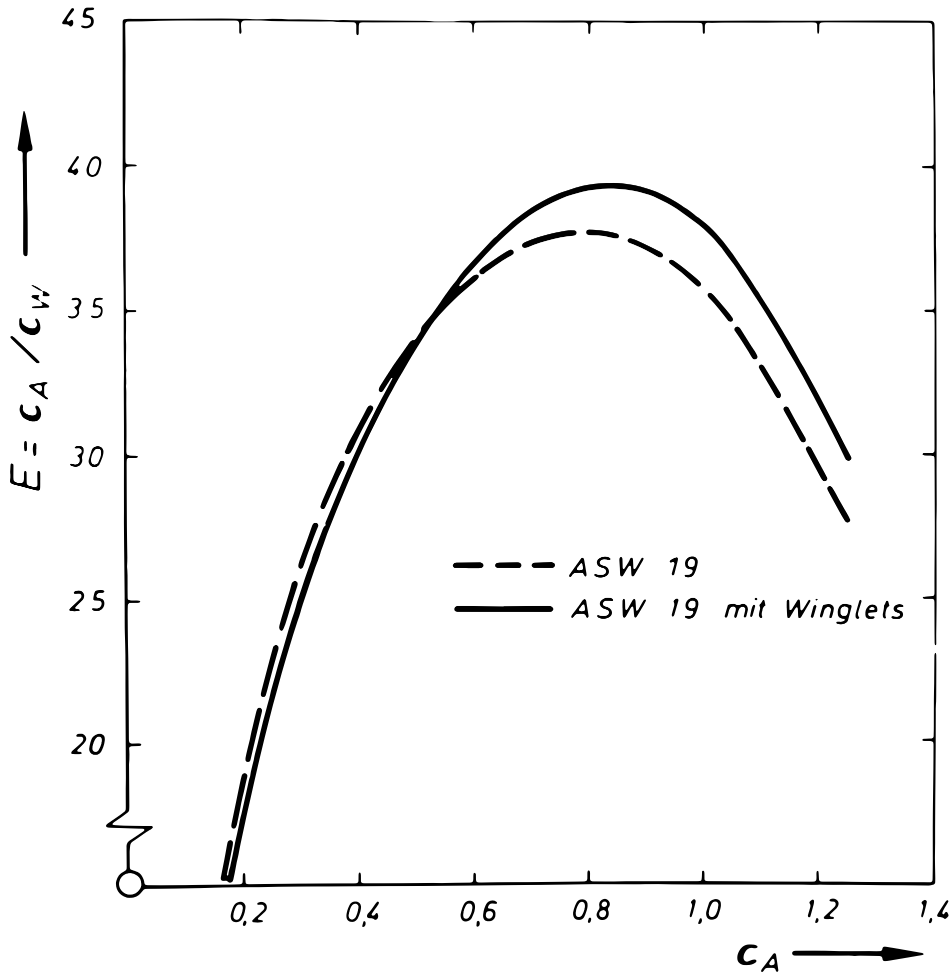

Figure 1.1. L/D of Akaflieg Braunschweig's ASW-19 with 1-meter-tall winglets compared to the unmodified ASW-19. Lift coefficient is on the x-axis and sailplane L/D is on the y-axis. Figure from Ref. [1].

Despite these setbacks, engineer and competition sailplane pilot Peter Masak was convinced that the profile drag penalty of winglets in cruise could be successfully mitigated on a sailplane [16]. Masak enlisted the help of Dr. Mark Maughmer, and although little was understood about the operating conditions of a sailplane winglet, a new airfoil, the PSU 90-125, was designed in a first attempt to understand this regime. This airfoil attempted to minimize profile drag at low lift coefficients and perform well across a broad range of Reynolds numbers. Masak and Maughmer proceeded to constrain the winglet design space through trial and error, experimenting with changes in cant angle,

Figure 1.2. Modern competition sailplanes with winglets. This photo is taken from an 18-meter Schleicher ASG-29, and the sailplane visible nearby is an 18-meter Schempp-Hirth Discus 2cT. Photo by Noah Reitter.

sweep angle, winglet root chord size, twist distribution, taper ratio, and finally, toe angle. Although winglets were initially viewed with hesitance and suspicion within the competition soaring community, the top five places in the 1991 15-Meter World Championships went to gliders equipped with winglets [16]. Further contest success and favorable pilot opinion eventually led to their widespread acceptance and implementation on both existing sailplanes and factory-new designs (as shown in Figure 1.2).

1.5 Previous Research in Adaptive Winglet Design

As the design tools have improved and the winglet design space has become better understood, the idea of changing winglet geometry in-flight has become increasingly popular for aerodynamic, control, and structural benefits.

The ideas presented in this thesis are revisited from a variable-toe winglet concept

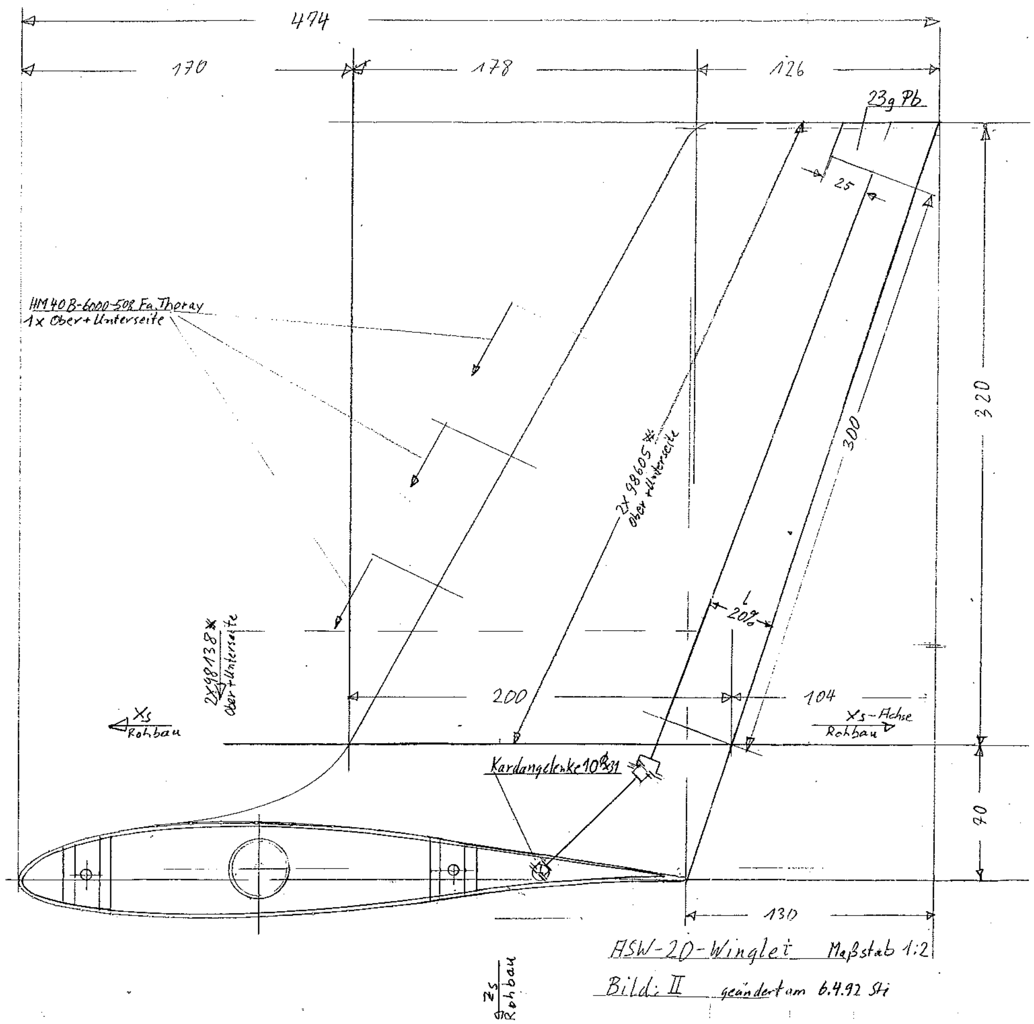

Figure 1.3. Gerhard Stichling's flapped winglet concept for the Schleicher ASW-20. Reproduced with permission.

pursued in the mid 2000s for the Schempp-Hirth Nimbus 4. These winglets were designed by Dr. Mark Maughmer and built by Monty Sullivan and Heinz Weissenbuehler[1]. Weissenbuehler intended to compete with them in the 2008 World Gliding Championships, but the project was never completed. These winglets used hinges located within the winglet junctures to set the toe angle for climb or for cruise. Model airplane servos actuated the winglets from a switch in the cockpit, and flexible membranes covered the resulting gaps in the winglet junctures. A more recent design study by Malinowski investigated morphing winglets on the Schempp-Hirth Ventus 2ax using fully-turbulent

[1]Because this project was never completed or published, the descriptions of variable-toe winglets for the Schempp-Hirth Nimbus 4 given in this thesis result from detailed conversations the author has had with Maughmer, Weissenbuehler, and Sullivan.

Reynolds-averaged Navier-Stokes computational fluid dynamics simulations [17]. Despite these limitations, the tested geometry generated "small, but not negligible" improvements in performance.

In the mid 1990s, Deutsches Zentrum für Luft- und Raumfahrt (DLR) test pilot Gerhard Stichling designed and flight-tested flapped winglets for his Schleicher ASW-20. Stichling's winglets incorporated aerodynamic and mass balances at the outboard end of the flap and an actuating servo in the sailplane wing tip. It is not clear how well Stichling's winglets worked, as they were designed just before the winglet design space was well-enough understood for such an effort to intentionally produce meaningful gains. Nonetheless, his idea is inspiration for some of the work pesented herein. Stichling's winglet is presented in Figure 1.3.

For larger aircraft, the aerodynamic gains created by winglets combined with active load alleviation provided by control surfaces located on the winglets is particularly appealing. This is because the supplemental structural weight required to support the additional bending loads applied by winglets on larger aircraft begins to negate the aerodynamic benefits of the winglets themselves.

Tamarack Aerospace Group, Inc. has designed, tested, and certified a combination of wing extension and winglet for the Cessna Citation CJ series and the Beechcraft King Air 200 and 350 [18, 19]. Tamarack's "SMARTWING" modification is marketed as an "active winglet," and although Tamarack's patent includes a control surface on the trailing edge of the winglet, their current installations include a trailing edge device only on the wing extension. This flap deflects autonomously to unload the outer wing section when a gust is encountered or the load factor is otherwise increased. Tamarack claims their modification extends range, reduces fuel consumption, and improves takeoff and climb performance.

In 2007, Boeing filed a United States patent for "controllable winglets" intended for commercial transport aircraft and other flight vehicles [20]. Generally, Boeing's patent incorporates shape memory alloys into a blended winglet. Cant, toe angle, and a control surface on the trailing edge of the winglet can be adjusted by a winglet flight computer to improve aerodynamics throughout the performance envelope of the aircraft, reduce wingspan for ground operations, and to perform gust alleviation.

In Europe, Wildschek et al. investigated similar design optimization of "active winglets for loads alleviation" for commercial transport aircraft [21]. This study proposes a certifiable control system that moves a tab on the winglet trailing edge to reduce wing bending loads. The aerodynamic benefits of winglets are not explicitly quantified in this study; however, the authors believe that the proposed installation could enable winglet retrofits on certain operational aircraft types without strengthening their outer wing structure. Similarly, Dimino et al. have designed full-scale morphing winglets for a regional airliner as part of the European Union's collaborative Clean Sky 2 Project [22]. This investigation used configuration-level computational fluid dynamic simulations to predict the performance benefits of coupled morphing wing/winglet combinations. It was determined that the aircraft with morphing structures had as much as a 3-percent drag reduction in climb compared to the baseline configuration with fixed winglets while also benefiting from active load alleviation. The Clean Sky 2 Project will test an adaptive winglet/wing on a modified Airbus C295 demonstrator aircraft.

Other academic and industry studies have been conducted to explore the benefits of variable winglets as well [23–25]. Bourdin et al. used a vortex lattice model and wind tunnel testing to determine that adjusting winglet cant in-flight can successfully control yaw, pitch, and roll of a model flying wing [26]. Falcao et al. used a multi-disciplinary optimization approach to quantify the performance benefits of an adaptive wingtip designed for a small unmanned aerial vehicle [27]. They conclude that their proposal has "significant potential," particularly for reducing aircraft stall speed and improving takeoff/landing performance. Eguea et al. coupled an optimization algorithm with a full potential/3D boundary layer solver to design camber morphing winglets for a mid-size business jet [28]. They conducted a wind tunnel campaign to validate their computational results, and concluded that their camber-morphing winglet reduces the total drag of the aircraft up to 0.58% over the baseline aircraft with fixed winglets.

1.6 Research Goals

The goal of the research report herein is to complete the preliminary aerodynamic design of variable-toe winglets for a modern competition sailplane, and to conceptualize strategies to realistically implement them. This entails:

1. Scheduling the winglet position and flap setting throughout the sailplane flight envelope to maximize the sailplane performance.

2. Quantifying these achievable performance gains and understanding their specific causes.

3. Contextualizing these gains in relation to soaring contests and other possible sailplane modifications.

4. Considering strategies to most effectively and realistically accomplish these gains in flight.

It is the author's hope that this work will facilitate a sailplane with variable-geometry winglets to be successfully flight tested in the near future.

Chapter 2 Fundamentals of Sailplane Performance

2.1 Forces in Cruising Flight

At its core, performance optimization is the intentional modification of the forces acting on an aircraft. Forces acting over distances result in work performed or energy stored, so aircraft trajectories are most basically aerodynamic forces applied to altitude and range. In this process, the designer will separate the balance of forces into components: lift, drag, thrust, and weight. It is tempting to treat these as individual properties that can be separately tailored to improve aircraft performance; however, aircraft design is about embracing the aircraft as more than a point mass. These forces are fundamental, coupled properties of aircraft configuration, and even seemingly-inconsequential decisions like paint color will, in some way, impact the balance of these forces. Therefore, the sailplane designer will attempt to make an aircraft as light and as aerodynamically-clean as possible while recognizing that reducing drag will inevitably affect lift and weight, and so on. The art of aircraft design is about making graceful, intentional compromises. With this context in mind, the basics of sailplane performance will now be explained.

As illustrated in Figure 2.1, a sailplane in steady, level flight is acted upon by three longitudinal forces in equilibrium: lift, drag, and weight. Lift enables flight. It is primarily generated by the wing and acts perpendicular to the sailplane velocity vector. Drag and weight are nemeses of the aircraft designer. Drag directly opposes the sailplane velocity vector, impeding the motion of the aircraft. Weight pulls the sailplane towards the center of the Earth. Fundamentally, lift and drag are defined with the freestream density ρ, the freestream velocity V, and the wing area S. The aircraft lift coefficient, C_L, and the aircraft drag coefficient, C_D, are non-dimensional parameters that depend on both the

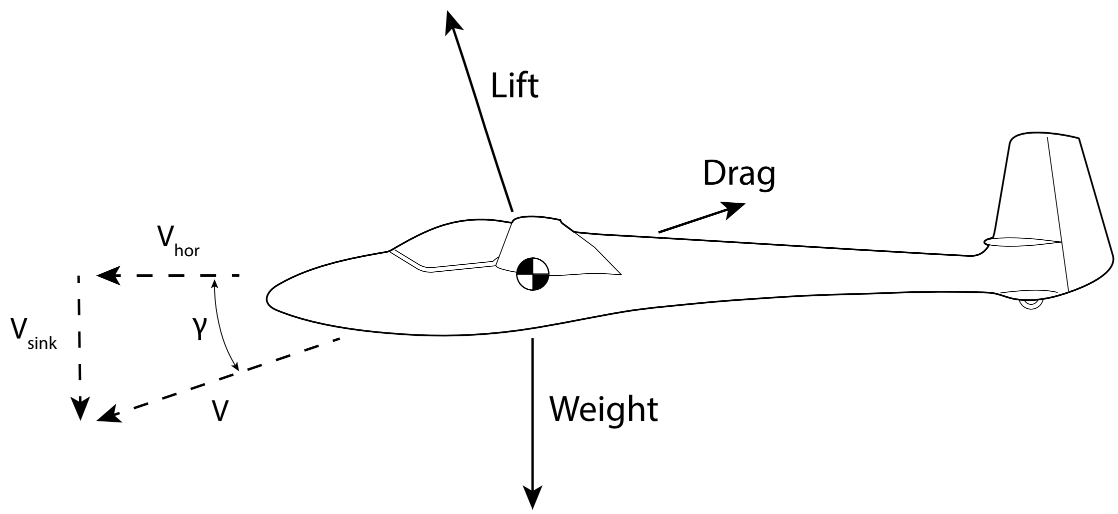

Figure 2.1. Fundamental forces acting on a sailplane in trimmed, cruising flight.

aircraft geometry and the state of the flowfield. Weight is defined with the sailplane mass m and the gravitational acceleration g. The flight path angle γ is the angle between the aircraft velocity vector and the horizon.

$$L = \frac{1}{2}\rho V^2 S C_L \tag{2.1}$$

$$D = \frac{1}{2}\rho V^2 S C_D \tag{2.2}$$

$$W = mg \tag{2.3}$$

Since lift, drag, and weight must balance for the sailplane to remain unaccelerated, the horizontal and vertical forces can be written:

$$\sum F_x : \quad L \sin\gamma = D\cos\gamma, \tag{2.4}$$

$$\sum F_z : \quad L\cos\gamma + D\sin\gamma = W. \tag{2.5}$$

It is immediately apparent that a sailplane with no means of propulsion must overcome its drag by tilting its lift vector in the direction of its flight. Lift then has two substantial roles: balancing weight and opposing drag. The sailplane horizontal velocity V_{hor} and sink rate V_{sink} can also be related to the flight path angle:

$$\tan\gamma = \frac{V_{sink}}{V_{hor}}. \tag{2.6}$$

Equations (2.5) and (2.6) can be combined to formulate the sailplane glide ratio:

$$\frac{L}{D} = \frac{V_{hor}}{V_{sink}}. \tag{2.7}$$

If the flight path angle is sufficiently small, lift is nearly equal to weight and V_{hor} is nearly equal to V. The glide ratio can then be approximated:

$$\frac{W}{D} = \frac{V}{V_{sink}}. \tag{2.8}$$

The glide ratio is a useful benchmark of aircraft efficiency because it directly compares the amount of the useful lift generated by the wing to the detrimental realities of drag. The larger it becomes, the farther the aircraft can glide. Typical maximum L/D for sailplanes ranges from 20 to 60. Since lift is nearly equal to weight in trimmed flight, the primary mission of the aircraft designer is clear: reduce drag as much as possible, and make the C_L range as wide as possible.

The glide ratio is uniquely defined for every flight condition the aircraft experiences throughout its design speed range. A sailplane must achieve the highest performance both while flying slow (as it climbs in thermals) and flying fast (as it cruises between them). Therefore, the designer must accomplish the challenging task of both expanding the flight envelope and improving the sailplane over its entirety. It then becomes necessary to express sailplane turning performance so it too can be understood and maximized.

2.2 Forces in Turning Flight

As illustrated in Figure 2.2, the turning performance of a sailplane can be approximated by modifying the previously-derived cruise equations by bank angle ϕ. Once again, γ is assumed to be sufficiently small. The vertical force balance in Equation (2.5) becomes

$$L \cos\phi = W. \tag{2.9}$$

The lift now must overcome weight, oppose drag, and provide the necessary radial force to turn the sailplane. Consequently, the sailplane sink rate will increase in a turn. This can be expressed by modifying Equation (2.7):

$$\frac{L\cos\phi}{D} = \frac{V}{V_{sink}} \quad \Rightarrow \quad V_{sink} = V\frac{D}{L\cos\phi}. \tag{2.10}$$

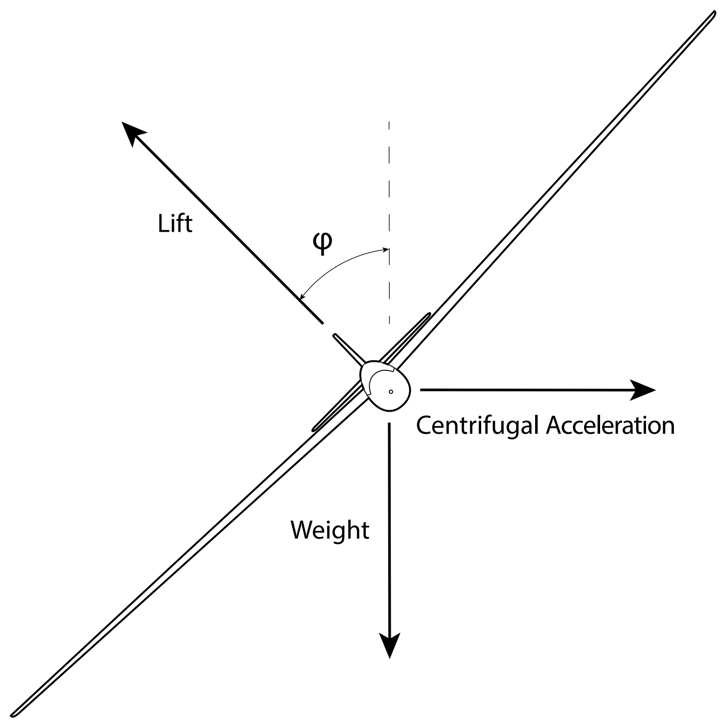

Figure 2.2. Fundamental forces acting on a sailplane in turning flight.

Using the definitions of lift and drag in Equations (2.1) and (2.2), the expression for V_{sink} in Equation (2.10) can be rewritten

$$V_{sink} = \frac{C_D}{C_L^{3/2}} \frac{1}{\cos^{3/2}\phi} \sqrt{\frac{2}{\rho}\frac{W}{S}}. \tag{2.11}$$

Additionally, the circling radius of the turning sailplane can be derived as a function of its tangential velocity V and bank angle ϕ using $\frac{mV^2}{R}$, the centripetal force required to turn an object:

$$R = \frac{V^2}{g \tan\phi}. \tag{2.12}$$

Equations (2.11) and (2.12) fundamentally model the thermaling performance of a sailplane by connecting its sink rate, turn radius, bank angle, and tangential velocity. To achieve the best climb rate in a thermal, a sailplane must stay within the strongest lateral bounds of the updraft with the smallest sink rate possible. This leaves the pilot with the task of choosing the best combination of V and ϕ to determine V_{sink} and R for a given thermal strength distribution and radius. Likewise, the sailplane designer must make V_{sink} as small as possible for even the narrowest thermals.

It is apparent from Equations (2.7) and (2.11) that $\frac{C_L}{C_D}$ must be maximized throughout the cruising envelope of the sailplane and $\frac{C_D}{C_L^{3/2}}$ must be minimized throughout the climbing envelope of the sailplane. To fully understand the impacts of these parameters on the effectiveness of a sailplane in soaring flight, they must be incorporated into a relevant trajectory that encompasses the entirety of the sailplane mission. The average cross-country speed will be used for this purpose.

2.3 Average Cross-Country Speed

A pilot flying a racing task strives to complete the course with the fastest average speed. This is a complex problem with many factors, including the sailplane performance, the airplane-handling skills of the pilot, the lines chosen through the sky, the consistency of the weather, and even random chance. These are pillars of a singular goal, which is to most efficiently use the energy stored in the altitude and airspeed of the sailplane. Every decision the pilot makes will impact the sailplane energy state for the remainder of the flight, so it is crucial to manage airspeed and altitude intentionally and most efficiently. One such approach is with MacCready's speed-to-fly theory [29].

MacCready's theory assumes that the climbing and gliding segments of a cross-country flight are distinct, and that the weather is uniform enough for the pilot to correctly predict the strength of the next thermal. Since the climb rate is known, the pilot can choose a cruise speed that optimizes the sailplane energy state when arriving at this next thermal.

Figure 2.3 graphically depicts the possible outcomes of different cross-country tactics. The first pilot is too conservative, wasting time to climb in weak lift at every opportunity. The second pilot is too aggressive, reaching the strongest thermal quickly, but too low to regain the altitude lost in the glide. The third pilot has flown too slow, wasting precious time gliding to the thermal. The fourth pilot has managed energy most effectively: flying fast enough in cruise to reach the strongest climb quickly, but reaching it with sufficient height to minimize the amount of time spent regaining altitude. The proper speed to fly for a given climb rate can be determined graphically from the sailplane straight-flight polar, and can be corrected for headwinds and sink. Thus, MacCready's theory guides sailplane pilots to optimally manage airspeed and altitude throughout a soaring flight. It is also useful for assessing the effectiveness of a sailplane for its fundamental mission: cross-country flight.

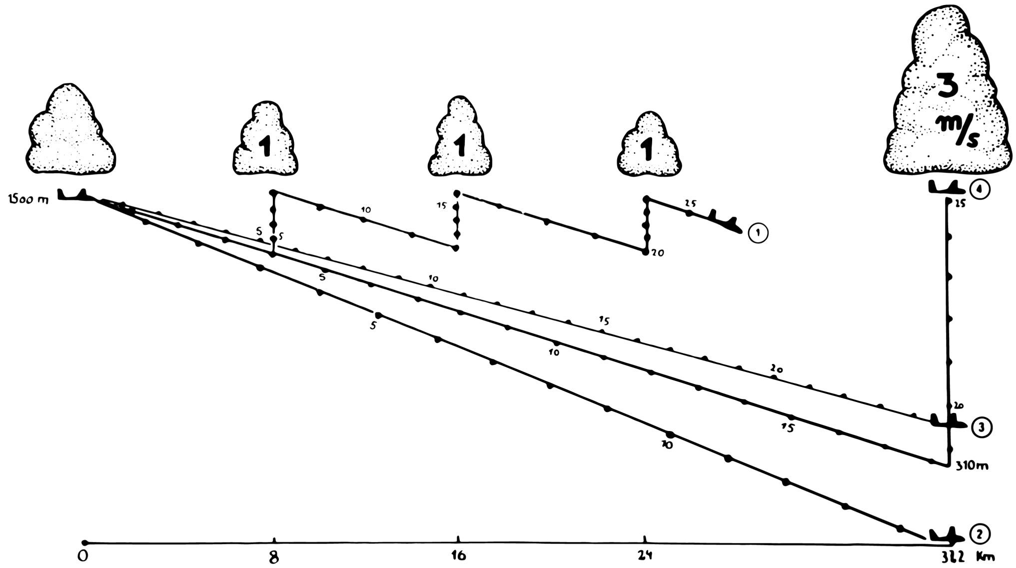

Figure 2.3. Impact of properly-selected inter-thermal cruise speed. Figure adapted from Ref. [2].

For the purpose of this work, the resulting average cross-country speed for a given thermal strength conveniently incorporates the sailplane straight-flight performance and climbing performance into one characteristic benchmark of its effectiveness for cross-country racing. It is a meaningful and consistent way to compare different sailplane configurations, even though it does not resolve tactics like ridge soaring or climbing in lift lines. The average cross-country speed will be derived below, but further extensions of MacCready's theory can be found in Ref. [2].

A simplified leg of a cross-country thermal flight is shown in Figure 2.4. First, the sailplane expends altitude h as it glides distance d at speed V_{cruise}. The cruising sink rate V_{sink} is determined by the straight-flight drag polar. The sailplane then thermals to regain altitude h at climb rate V_{climb}. The average cross-country speed of the sailplane, V_{acc}, can be expressed in terms of the time cruising, t_{cruise}, and the time climbing, t_{climb},

$$V_{acc} = \frac{d}{t_{climb} + t_{cruise}}. \tag{2.13}$$

The length of the glide and the cruise speed determine t_{cruise},

$$t_{cruise} = \frac{d}{V_{cruise}}. \tag{2.14}$$

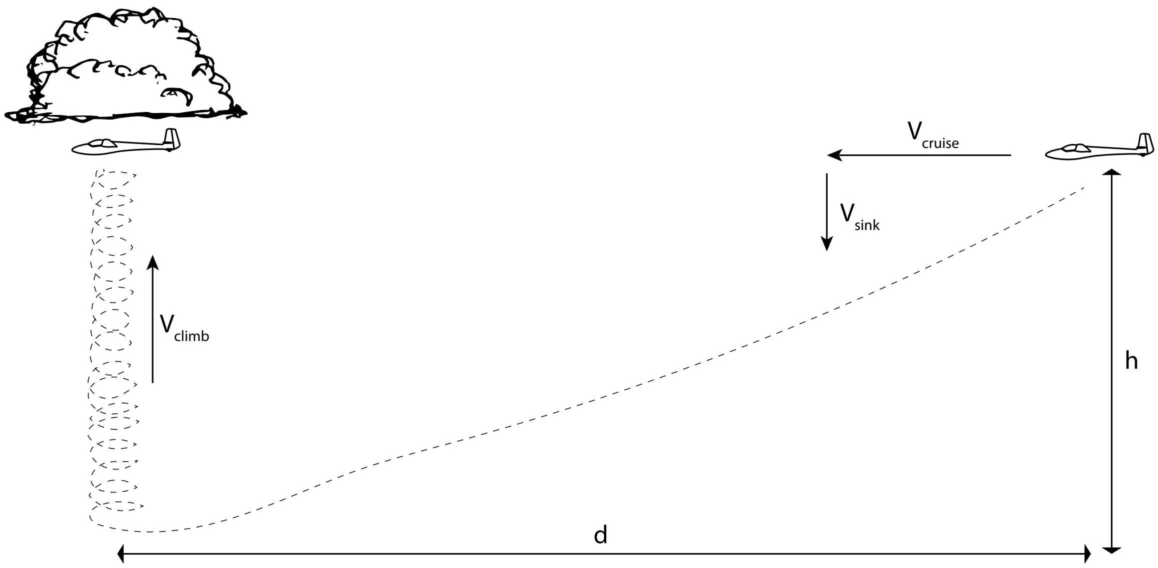

Figure 2.4. Portion of a thermal cross-country flight consisting of a gliding segment and a climbing segment.

Likewise, the height of the climb and the climb rate determine t_{climb},

$$t_{climb} = \frac{h}{V_{climb}}. \tag{2.15}$$

Since the sailplane descends altitude h during its cruise, h can be expressed in terms of t_{cruise} and V_{sink},

$$h = t_{cruise} V_{sink}. \tag{2.16}$$

The average cross country speed can be expressed in terms of V_{climb}, V_{sink}, and V_{cruise} by first substituting Equation (2.16) into Equation (2.15). The resulting equation and Equation (2.14) are then substituted into Equation (2.13):

$$V_{acc} = \frac{V_{cruise}}{V_{sink}/V_{climb} + 1}. \tag{2.17}$$

The maximization of Equation (2.17) provides the optimum average cross-country speed for a sailplane flying within a given set of thermal conditions. To accomplish the highest average cross-country speed, the sailplane designer must combine a high cruise speed with a low cruise sink rate while also achieving the highest possible thermalling climb rate. Fundamentally, this requires reducing the sailplane drag both in cruise and in

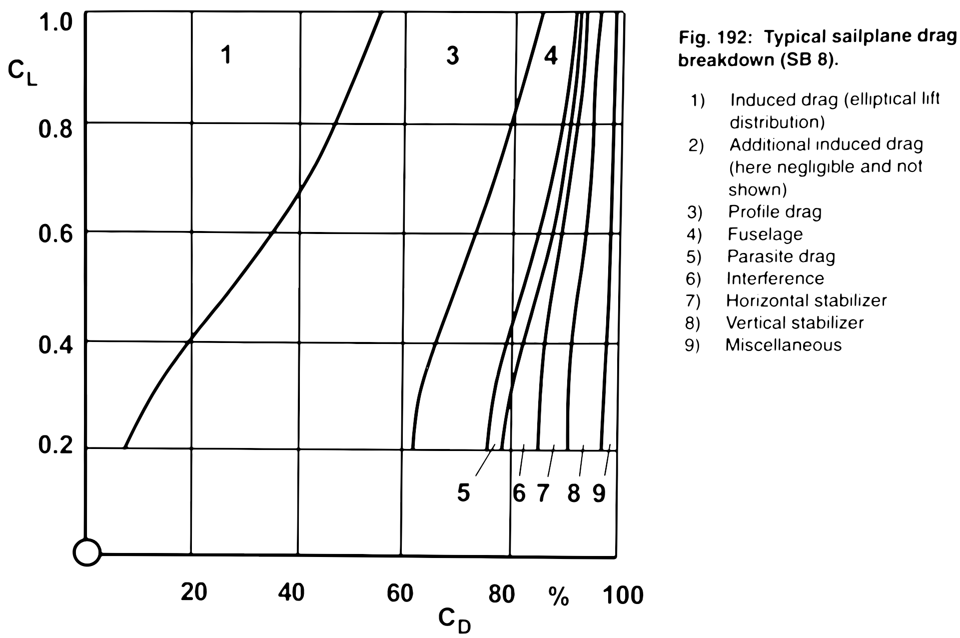

Figure 2.5. Contributions of various sailplane components to the sailplane total drag. Figure included from Ref. [3].

climb.

2.4 Drag on a Sailplane Wing

Competition sailplanes intentionally remove many of the aerodynamic inefficiencies that contribute significantly to the drag of other similarly-sized aircraft. Sailplane wings are cantilevered without external bracing, and exploit laminar-flow airfoils and optimized planforms. The fuselage is as small and as streamlined as possible. The main landing gear retracts into the fuselage and antennas are mounted internally. Gaps are sealed with mylar, tape, or foam. The structure is composite, and the surface finish is polished and free from rivet heads or other imperfections. All of these design decisions culminate in highly efficient vehicles. Because sailplanes are so aerodynamically clean, their wings contribute greater than half of the aircraft total drag in both cruise and climb (as shown in Figure 2.5), and reducing the drag of the wing tangibly improves the overall performance of the vehicle. Thus, reducing wing drag is the focus of this work.

2.4.1 Profile Drag of a Wing

Neglecting compressibility effects, the profile drag of a wing is a consequence of viscosity. It is strongly a function of the Reynolds number:

$$Re = \frac{\rho V c}{\mu}. \tag{2.18}$$

The Reynolds number is a non-dimensional parameter that varies with the freestream density ρ, the freestream velocity V, and the freestream dynamic viscosity μ. For aircraft, the reference length c is typically the wing chord. Conceptually, the Reynolds number compares the relative importance of the inertial properties of the flow (the numerator) with the viscous properties of the flow (the denominator). Typical flight Reynolds numbers of a sailplane range from 30,000 (winglet tip at stall speed) to 4,000,000 (wing root at maximum speed). Within this range of Reynolds numbers and at typical sailplane lift coefficients, the effects of viscosity are confined to a thin boundary layer adjacent to the body. The Reynolds number is a strong determinant of the location at which the boundary layer will transition from laminar to turbulent. The profile drag is composed of skin friction and pressure drag, both of which strongly depend on this boundary layer behavior.

2.4.1.1 Skin Friction Drag

The average flow velocity immediately adjacent to the surface of a wing is zero. The flow velocity increases across the height of the boundary layer from this "no-slip" condition at the surface to the local edge velocity. This vertical velocity gradient adjacent to the wall gives rise to shear stress that removes kinetic energy from the flow. If the boundary layer is laminar, the flow travels in smooth streamlines parallel to the surface without inertial mixing between layers. If the boundary layer is turbulent, eddies mix lower-momentum air away from the surface and higher-momentum air towards the surface. This turbulent mixing improves the separation resistance of a turbulent boundary layer. Consequently, a turbulent boundary layer has significantly more skin friction than an equivalent laminar boundary layer because of the increased wall shear stress of the larger velocity gradient near the body, as shown in Figure 2.6. Thus, sailplane airfoils attempt to achieve the longest laminar runs possible before cleanly undergoing transition. This compromise combines the lower skin friction drag of a laminar boundary layer with the higher separation resistance of a turbulent boundary layer.

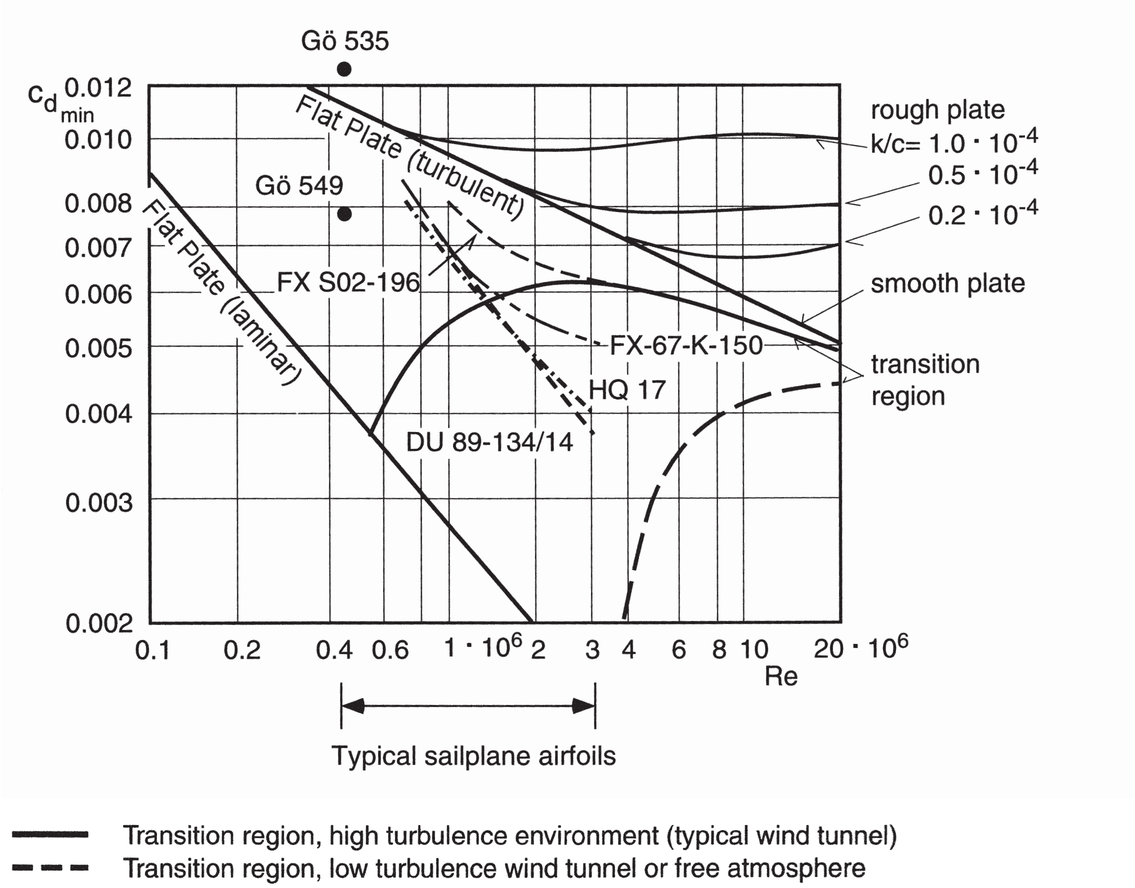

Figure 2.6. Skin friction drag coefficient plotted as a function of Reynolds number for a two-sided flat plate. The minimum drag coefficients of some typical sailplane airfoils are included for reference. Figure adapted from Ref. [3].

2.4.1.2 Pressure Drag

The momentum deficit near the wall also causes a loss in total pressure throughout the boundary-layer development, which generates a pressure gradient force on the body in the drag direction. While this pressure drag is usually small at low angles of attack, it comprises a substantial portion of the profile drag at higher angles of attack, especially if the boundary layer begins to separate. Separation occurs when skin friction and an adverse streamwise pressure gradient sufficiently remove momentum from the near-body flow. This usually occurs at high angles of attack (typically encountered when a sailplane is climbing or landing). Once a boundary layer separates, the static pressure on the surface can no longer recover to its freestream value. Resisting separation is crucially important because the pressure drag generated by a separated boundary layer will almost

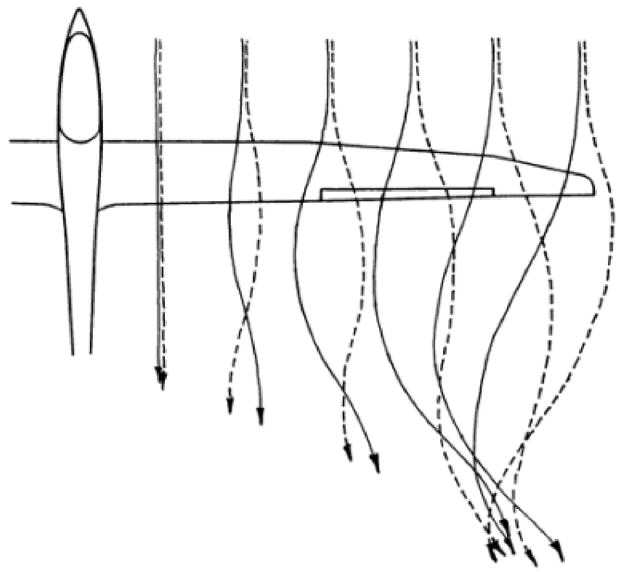

Figure 2.7. Spanwise shearing of flow over a finite wing. Figure from Ref. [4].

always be more substantial than skin friction drag caused by a turbulent boundary layer. This is also why sailplane designers work so hard to limit external protrusions of structural bracings, antennas, and landing gear.

2.4.2 Induced Drag of a Wing

A wing generates lift by enforcing a pressure differential between its upper and lower surfaces. This pressure differential changes the momentum of the flow; the wing accelerates some of the air that it encounters downwards, which reacts to support the weight of the aircraft. Unfortunately, the pressure difference between the two surfaces of the wing also has undesirable effects: spanwise pressure gradients are generated at the wingtip by the interaction between the high-pressure air on the bottom surface and low-pressure air on the top surface. These pressure gradients generate velocities that pull air outboard on the lower surface and inboard on the upper surface, as illustrated in Figure 2.7. Vorticity is generated by the spanwise shearing of flow, which is shed at the wing trailing edge. In subsonic aerodynamics, the state of every point within a flowfield depends on the states of every other point. Thus, the shed vorticity influences the wing downwash field and lift distribution, and vice versa. The resulting deformation of the flowfield reduces the lifting efficiency of the wing, and this is called induced drag. The relative importance of this entire process is directly related to the angle of attack: at high angles of attack, the pressure difference between the top and bottom surfaces of the wing is the greatest. Therefore, the spanwise pressure gradients are strongest, the flowfield is most deformed, and the induced drag is the highest.

2.5 Formulation of Drag on a Sailplane Wing

The total drag of a sailplane wing at a given lift coefficient can be written as a sum of the wing profile drag and induced drag,

$$D_{wing} = D_{profile} + D_{induced} = \frac{1}{2}\rho V^2 S C_{D_{profile}} + \frac{1}{2}\rho V^2 S C_{D_{induced}} \tag{2.19}$$

The profile-drag coefficient of an airfoil is the sum of the pressure and skin friction drag coefficients,

$$c_d = c_{d_{friction}} + c_{d_{pressure}}. \tag{2.20}$$

The profile-drag coefficient is a strong function of angle of attack and Reynolds number. For laminar-flow airfoils, there is a range of lift coefficients in which the profile-drag coefficient is at its minimum and is approximately constant. This low-drag range corresponds to the angles of attack at which significant runs of laminar flow extend over both the top and bottom surfaces of the airfoil. If the spanwise lift distribution is known for a wing at a given angle of attack, strip theory or a table look-up method can be used to average the section profile-drag coefficient at each spanwise station (c_d) into the total profile-drag coefficient for the entire wing ($C_{D_{profile}}$):

$$C_{D_{profile}} = \int_{-b/2}^{b/2} c_d(y)dy. \tag{2.21}$$

Likewise, the induced drag coefficient C_{Di} for a wing can be expressed in terms of the wing's span b and its planform efficiency factor e:

$$C_{D_i} = \frac{C_L^2}{\pi e}\frac{S}{b^2}. \tag{2.22}$$

The quantity $\frac{b^2}{S}$ is the wing's aspect ratio, AR. The planform efficiency factor e quantifies the wing deviation from elliptical loading. For typical high performance sailplanes, e ≈ 1, and is approximately constant for the normal operating range of lift coefficients. It can be determined more precisely using a finite-wing code. For a specific sailplane geometry, Equation (2.22) can be dimensionalized and simplified with Equation (2.1):

$$D_{induced} = \frac{1}{2}\rho V^2 S \frac{C_L^2}{\pi e AR} = \frac{2}{\pi \rho e}\left(\frac{L}{b}\right)^2 \frac{1}{V^2}. \tag{2.23}$$

Finally, Equation (2.19) can be rewritten with Equation (2.23):

$$D_{wing} = \frac{1}{2}\rho V^2 S C_{D_{profile}} + \frac{2}{\pi \rho e}\left(\frac{L}{b}\right)^2 \frac{1}{V^2}. \tag{2.24}$$

Crucially, Equation (2.24) provides an intuitive relationship for the wing total drag as a function of the flight speed V. Although the profile-drag coefficient is a function of both lift coefficient and Reynolds number (and thus V), it is evident that profile drag primarily grows rapidly with V^2. Conversely, the induced drag dominates at low speeds, but rapidly diminishes with V^2. In steady, level flight, the speed at which the induced drag is equal to the profile drag is the speed at which the aircraft achieves its maximum L/D.

2.6 Fundamentals of Winglets

Winglets reduce induced drag by using aerodynamics to modify the wingtip pressure gradients and reduce spanwise flow. A wing with winglets behaves as if it has the induced drag of a wing with a larger span, and this change is quantified by an increase in span efficiency e. Unfortunately, the addition of winglets to a sailplane also adds wetted area, which increases the profile drag of the wing. Effective winglets reduce induced drag with the smallest possible penalties in profile drag. Arriving at this compromise is especially challenging for a sailplane because they must excel in cruise at high speed/low lift coefficients (which amplifies profile drag penalties) while also maintaining maximum climb rates at slow speeds/high lift coefficients (which winglets most benefit).

2.6.1 The Winglet Design Problem

The first production sailplane winglets were designed using the crossover point method described by Maughmer and Kunz in Ref. [30]. This method explicitly balances the induced drag improvements caused by winglets at low speeds with the accompanying increases in profile drag at high speeds. The speed at which the drag benefits are equal to the losses is the crossover point. When a sailplane with winglets flies slower than this

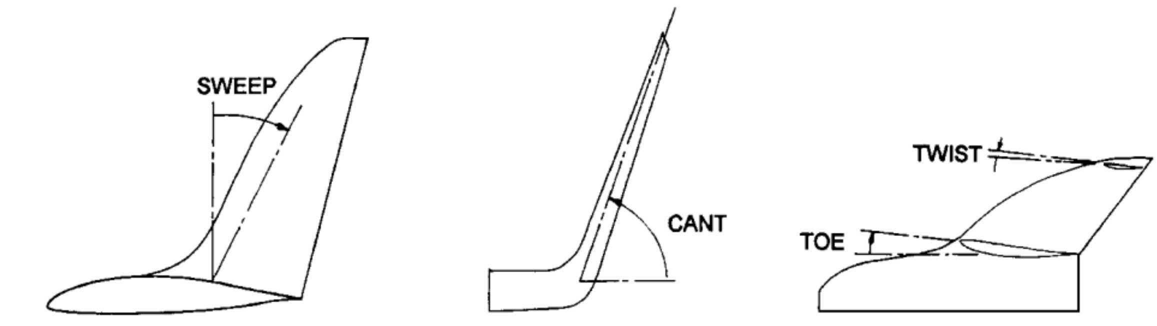

Figure 2.8. Properties of winglet geometry that can be tailored for design. Figure adapted from Ref. [5].

speed, it outperforms an equivalent sailplane without winglets. However, as the sailplane cruises faster than the crossover point, the profile drag penalties become substantial and its performance degrades below that of the unmodified sailplane. Although these winglets were successful when operated entirely below the crossover point, high-speed cruise performance was significantly penalized. This was particularly problematic when cruising between strong climbs, dolphin-flying within extended lift lines, or ridge soaring. Consequently, newer winglets are designed to reduce the cruising profile drag penalties. Tailoring the winglets to minimize high-speed losses reduces the potential climb benefits provided by winglets; however, the overall design improves performance more uniformly throughout the sailplane flight envelope.

2.6.2 Winglet Geometry

The established winglet design techniques incorporated into this thesis have successfully improved the performance of new and existing sailplanes alike, and are presented in Refs. [5, 16, 30]. Other techniques are not considered in this writing. The following geometric constraints are illustrated in Figure 2.8, and are considered purely from their aerodynamic importance to a sailplane. Structural implications (such as the winglet contribution to the root bending moment) and manufacturing feasibility must also be incorporated into a successful winglet design.

2.6.2.1 Airfoil Selection

Winglets operate in a field of strong velocities induced by the spanwise pressure gradients of the main wing, and the strength of these pressure gradients depends on the sailplane angle of attack. Because of this, the winglet angle of attack primarily depends on the main wing angle of attack rather than the sailplane sideslip angle. The specific range of lift coefficients experienced by the winglet is unique to each individual wing/winglet combination, but the design goal remains: the sailplane winglet must produce the required lift with the least possible drag. This presents a unique design challenge: winglets are most beneficial in climb, so they must produce high lift coefficients when the main wing is near stall. At the same time, winglets must maintain low profile-drag coefficients in high-speed cruise, where their additional wetted area is most detrimental to sailplane performance. The range of Reynolds numbers over which these disparate operating requirements occur is especially difficult. The winglet tip can experience Reynolds numbers lower than 50,000 at the sailplane stall speed, and the winglet root can experience Reynolds numbers as large as 1,000,000 in high-speed cruise. Within this range, the profile-drag coefficient and the maximum lift coefficient strongly depend on the transition location and the mechanism of transition. Thus, the designer must achieve high maximum lift coefficients at very low Reynolds numbers while maintaining low profile-drag coefficients at low lift coefficients and higher Reynolds numbers. These are difficult compromises to make elegantly. The winglets modeled in this thesis were designed with the PSU 02-097 airfoil, which was tailored to the unique, previously-described needs of a sailplane winglet. Every wing/winglet combination is distinct, and ideally, every winglet would have its own, specifically designed airfoil. Fortunately, the operating regime of most sailplane winglets is similar enough for the small performance benefits of such an effort to be unnecessary, and the remaining geometry of the winglet can be adjusted to maximize the benefits of winglets for every sailplane. More information about winglet airfoil design can be found in Refs. [31, 32].

2.6.2.2 Cant Angle and Height

Winglet cant angle and height must be considered together in the winglet design process. Aerodynamically, winglet height is a familiar compromise between induced drag improvement and profile drag penalty: taller winglets provide more distance to smoothly shed vorticity but increase the wetted area. Practically, it has taken time for sailplane pilots to accept tall winglets. The first production winglets for the Schleicher ASW-24E were introduced in 1992, and were only 30 cm tall. Thirty years later, the Schleicher AS-33 leaves the factory with 60 cm winglets. Similarly, most Schempp-Hirth sailplanes (including the Ventus 2bx studied in this work) have 40 cm winglets, but the recent Ventus 3 has increased the winglet height to 49 cm. Cant angle is more consistently defined among sailplane winglets. The minimum cant angle is constrained by wing tip deflection. Composite sailplane wings are relatively flexible, with wing tips for some large-span sailplanes deflecting as much as 30 degrees when highly loaded. The winglet must have at least enough cant to avoid tilting inward at maximum wing tip deflection; otherwise, a component of the force generated by the winglet would work against the lift of the main wing. The maximum cant angle is constrained by the FAI class wingspan definitions. The winglet usually begins immediately outboard of the aileron, and the cant angle is established for the wing span to exactly equal to the class definition when measured between each winglet tip. This method also removes some of the original sailplane wing tip, which offsets some of the additional wetted area added by the winglet.

2.6.2.3 Winglet Planform Shape

Selecting the winglet chord presents an important profile drag compromise. The chord-lengths must remain small enough to minimize the wetted area of the winglet, while also large enough for the Reynolds number to stay above excessive profile-drag coefficient penalties [5]. The winglet planform is also coupled with the twist distribution and sweep angle to determine the winglet loading. This is a trade-off between chord-length and lift coefficient. If the chords are too small, the winglet lift coefficients are excessive, potentially beyond stall at low speeds. This is undesirable both because of the reduced effectiveness of a stalled winglet and by the excessive pressure drag it inflicts. Conversely, excessively large chords inefficiently under-load the winglet. This is equally undesirable because the larger chords increase the wetted area of the winglet without any benefit. Together, the chord distribution, twist, and sweep should be adjusted so that the winglet is loaded elliptically. The winglets assessed in this thesis were designed with an elliptical chord distribution, except near the tip to limit the leading-edge sweep.

2.6.2.4 Twist Distribution and Sweep Angle

Once the planform is fixed, twist and sweep act similarly to determine the winglet load distribution [16]. Because of the spanwise velocities at the wing tip, the local inflow angle at the base of the winglet is higher than at the tip. Thus, winglets are washed in to keep the c_l distribution approximately constant. Likewise, the spanwise velocities are strongest in the wake, so adding sweep increases the amount of lift produced towards the winglet tip. Excessive sweep must be limited to keep cross-flow instabilities from transitioning the flow prematurely. As designed currently, the winglet sweep is defined aesthetically for a given wing geometry, and the twist is adjusted to generate the proper spanwise loading. The winglets assessed in this thesis have approximately 2.5° of twist and 30° of leading-edge sweep.

2.6.2.5 Toe Angle

Setting the toe angle is the most consequential part of the winglet design process because it is the final determinant of the winglet loading throughout the sailplane flight envelope. Since the winglet angle of attack is tied directly to the angle of attack of the main wing, the toe angle chosen will only be truly correct for one flight condition. This is the crux of the winglet design compromise: increasing the toe angle increases the winglet loading and improves low-speed performance; however, it also increases the drag penalties at higher speeds. Therefore, it is the designer's job to select a toe angle that trades moderate gains in climb performance with marginal losses in cruise performance. Variable-toe winglets eliminate this compromise by adjusting the toe angle to be optimum at every flight condition, thereby minimizing the sailplane total drag.

2.7 Variable-Toe Winglets

The design compromises of a winglet become substantially easier to balance if the winglet geometry is allowed to vary throughout the sailplane flight envelope. The toe angle is the natural choice to change: it has the most significant effect on the sailplane performance and is relatively simple to alter in flight. Most of the geometric properties previously described are fixed either by practical necessity or by other requirements. A fixed winglet only enables the optimum span lift distribution at one lift coefficient. Variable-toe winglets allow the wing to achieve better span-lift distributions at multiple lift coefficients–as if the wing twist itself could be changed dynamically.

Chapter 3
Design Tools and Methods

3.1 Design Tools

Fundamentally, this thesis applies relatively simple tools to predict and analyze the performance of a sailplane configured with different flap settings and winglet toe angles. These tools are described below.

3.1.1 PGEN

Polar Generator (PGEN) is an in-house software package developed for rapidly assessing different sailplane configurations. Altogether, PGEN considers non-planar wing planforms, washout, multiple airfoils, flap scheduling, static margin, and different gross weights. PGEN uses text files that cover the overall geometry of the aircraft and the specific performance behavior of the airfoils it uses. It has been used for the design of sailplane winglets since its creation in the late 1990s, and it has been well validated for this task (as is shown in Figure 3.1). A brief summary of PGEN's performance routine is given below, but further description of the code can be found in Ref. [33].

3.1.1.1 Wing and Tail Lift

The first step of calculating aircraft drag at a given speed is determining the lift coefficients of the wing and the tail as required for the sailplane to trim with no net forces and moments about the center of gravity. The net forces are expressed in Equations (2.4) and (2.5). The net pitching moment about the center of gravity can be written as a sum of the pitching moment of the wing airfoil, the pitching moment of the fuselage, and the moments applied by the wing and tail lift forces acting at their respective distances from the center of gravity. The pure moment generated by the horizontal tail airfoil is

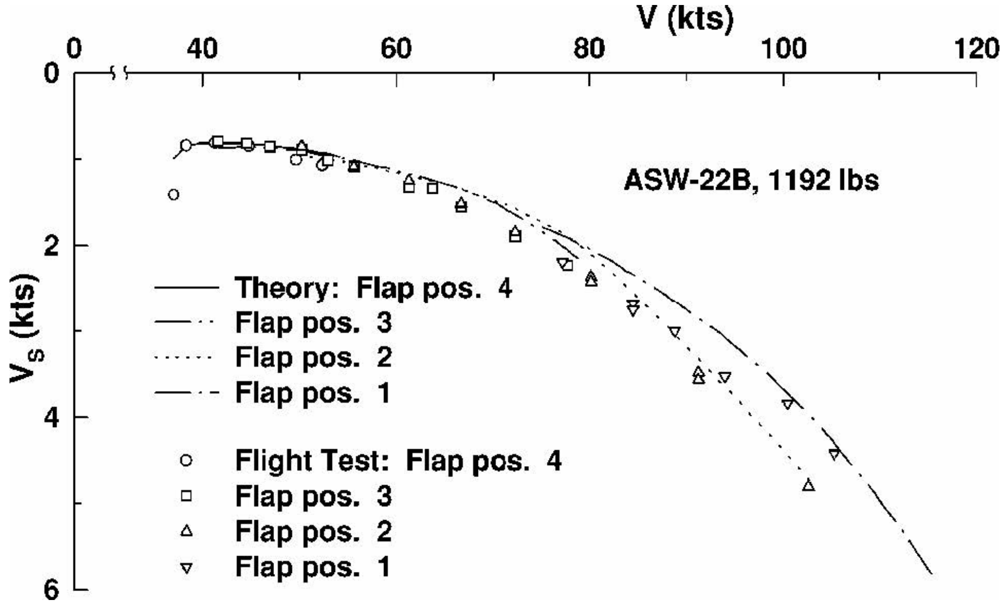

Figure 3.1. PGEN polar prediction for the Schleicher ASW-22 validated against flight-test data. Plot reproduced from Ref. [5].

comparatively small and can be neglected. In non-dimensional form, the total expression for the trimmed sailplane pitching moment coefficient about its center of gravity, $C_{M_{cg}}$, becomes:

$$C_{M_{cg}} = 0 = C_{L_w}\left(\frac{x_{cg} - x_{ac_w}}{\bar{\bar{c}}}\right) + C_{M_{ac_w}} + C_{M_{fuse}} + C_{L_{tail}}\frac{S_{tail}}{S}\left(\frac{x_{cg} - l_{tail}}{\bar{\bar{c}}}\right). \tag{3.1}$$

Here, the lift acts at the wing aerodynamic center, whose location is written as x_{ac}. This is convenient because the wing pitching moment coefficient about its aerodynamic center, $C_{M_{ac_w}}$, is constant with changes in the aircraft C_L for a given flap setting. Similarly, the fuselage pitching moment coefficient, $C_{M_{fuse}}$, can be written as a function of C_L. S_{tail} and S_{wing} are the aircraft tail area and wing area, respectively. l_{tail} is the distance between the center of gravity and the aerodynamic center of the tail, and x_{cg} is the location of the center of gravity. The wing mean aerodynamic chord, $\bar{\bar{c}}$, can be calculated by evaluating the integral,

$$\bar{\bar{c}} = \frac{1}{S}\int_{-b/2}^{b/2} c(y)^2 dy. \tag{3.2}$$

Equation (2.9) can be modified to incorporate the aircraft lift as a sum of the lift produced by the wing and the horizontal stabilizer:

$$\frac{W}{\cos\phi} = \frac{1}{2}\rho V^2 S C_{L_w} + \frac{1}{2}\rho V^2 S_{tail} C_{L_{tail}}. \tag{3.3}$$

Equations (3.1) and (3.3) are then solved simultaneously to determine the tail lift coefficient, $C_{L_{tail}}$, and the wing lift coefficient, C_{L_w}, required to trim at a given speed and flap configuration. Once these are known, Horstmann's multiple-lifting-line code is used to determine the wing spanwise lift distribution and span efficiency [33].

3.1.1.2 Horstmann's "LIFTING_LINE" Code

To determine the induced drag, PGEN implements Horstmann's higher-order, multiple-lifting-line code, which was developed to calculate the induced drag of nonplanar wings with comparable accuracy to lifting-surface programs [1]. Horstmann's code is computationally inexpensive, so it is well-suited to be called repeatedly and produce results rapidly [34]. Multiple-lifting-line methods substantially reduce the number of singularities required to represent complex geometries when compared to traditional vortex lattice methods. Horstmann's code separates the wing geometry into panels, which are further divided into tiles that contain vortex sheet elements with continuously-varying strength. Spanwise continuity is forced at the edges of each vortex sheet element for both the circulation magnitude and spanwise rate of change, and a "no-leaks" boundary condition is imposed for flow through the center span of each panel. The total lift is then calculated by integrating the circulation over the entire wing, and the induced drag is computed in the Trefftz-plane.

Horstmann's code allows for individual wing panels to be twisted relative to each other. This feature is used to implement flaps via twisting each panel by the zero-lift angle of the flapped wing section. The change in the zero-lift angle for each desired flap setting is included in the airfoil data files. This is the same method used to add washout or twist to other parts of the wing.

3.1.1.3 Profile Drag of the Wing and Tail

Once the lift distribution is known, it is used to determine the total profile drag of the wing. PGEN does this by discretely summing the local profile drag of each of the N

wing panels:

$$D_{p_{wing}} = \sum_{n=1}^{N} \frac{1}{2}\rho V^2 S_n c_{d_n}. \tag{3.4}$$

The lift distribution is used to determine the local c_l of each wing panel. Once this is known, it can be used along with the corresponding Reynolds number and flap setting to reference the local profile-drag coefficient of each panel, c_{dp_n}, from the airfoil data. PGEN uses an interpolation scheme to most accurately define the sectional characteristics at every Reynolds number and flap setting. This entire process can be repeated to account for the profile drag of the horizontal stabilizer.

3.1.1.4 Complete Drag Buildup

With the profile and induced drags of the wing known, the drag contributions of the rest of the aircraft must now be considered. The induced drag of the horizontal stabilizer can be computed using Horstmann's code the same way that the induced drag is determined for the main wing; however, for simplicity PGEN assumes the span efficiency of the horizontal stabilizer is 1.0. The entire induced drag of the combined wing/tail system is then calculated with Munk's Stagger Theorem and Prandtl's Biplane Equation.

The drag of the fuselage is accounted for by specifying its equivalent flat plate area, which includes any interference drag or other miscellaneous drags not explicitly defined elsewhere. This can also be used to "calibrate" the aircraft total drag. Once the sailplane total drag is properly compiled for the given flight condition, the L/D and sink rate can be computed. This whole process is then repeated for all desired flight conditions to build the sailplane straight-flight polar. The sailplane turning performance is obtained in a similar way.

3.1.1.5 Turning Performance

The most significant difference in determining the turning performance of a sailplane is that the total lift must now provide a radial force in addition to opposing the sailplane weight and drag. Thus, the total lift coefficient of the aircraft will increase proportionally to the desired turning force. The C_L required for the sailplane to achieve turn radius R with bank angle ϕ can be derived by combining Equations (2.1), (2.9), and (2.12) to give,

$$C_{L_{rqd}} = \frac{2W}{\rho g R S \sin\phi}. \tag{3.5}$$

PGEN generates turning polars by fixing the turn radius and determining which combination of ϕ and C_L minimize the sailplane sink rate (given by Equation (2.11)). PGEN does not consider the effects of aileron/rudder deflection or turn coordination, so the aircraft C_D at the required C_L is assumed to be the same value determined for straight flight.

3.1.1.6 ACCS Evaluator

The PGEN software package also includes an average cross-country speed (ACCS) evaluator that calculates the MacCready cross-country speed for a given sailplane. After PGEN outputs the straight-flight and turning polars, the ACCS program processes these data and generates cross-country speeds for a user-defined thermal radius as described by Equation (2.17). The ACCS evaluator assumes a parabolic distribution of updraft velocity within a thermal, and the sailplane maximum climb rate is determined by superimposing the turning polar onto the thermal updraft profile. Cross-country speeds are given for thermal core strengths up to 10 m/s. It should be noted that the sailplane's achieved climb rate is substantially lower than the thermal core strength because of the sailplane's required turn radius and sink rate.

3.1.2 Freewake

Freewake is an in-house code developed to predict the induced drag of non-planar wing geometries and combinations of wings [4]. It is conceptually similar to Horstmann's method, but Freewake allows the wake to relax. By shedding elemental vortex sheets rather than vortex filaments, Freewake eliminates the singular behavior that causes extreme velocities when two vortex filaments intersect. Thus, these discrete vortex elements can be combined to model a lifting surface that sheds a sheet of vorticity that is essentially continuous.

Freewake is used in this work as a supplement to the results supplied by Horstmann's code. Both methods provide similar results; however, Freewake considers the impact of the wake rollup on the lift distribution and span efficiency. These effects have been studied in Refs. [35–37] and are usually not very large; however, Freewake is a convenient tool to further understand the physical effects of variable-toe winglets on the sailplane lift distribution and induced drag throughout the flight envelope.

Flight Mass	Pilot Mass	Water Ballast	Nose Ballast	CG Position
330 kg	66 kg	0 kg	7 kg	0.353 m (98%)
525 kg	90 kg	176 kg	0 kg	0.282 m (94%)

Table 3.1. Aircraft weights and CG locations modeled in PGEN. The CG locations are expressed both in meters aft of the datum (which is the leading edge of the wing root) and percentages of the aft limit (which varies with sailplane mass) at each sailplane mass.

3.2 Sailplanes Analyzed

3.2.1 Schempp-Hirth Ventus 2bx

The Schempp-Hirth Ventus 2bx was selected as an appropriate configuration to assess in this thesis. It is representative of modern, 15-meter class competition sailplanes, and is a convenient choice because the advisor to this thesis owns one with an extra set of winglets that can be modified for flight test.

The Ventus 2bx is a 15-meter class competition sailplane designed and manufactured by Schempp-Hirth in Germany. Its structure is primarily composed of carbon fiber and fiberglass, and its published maximum L/D is 46. The Ventus 2bx considered in this thesis is serial number 162, N597MD, constructed in 2004. The specific winglets considered in this work are the first generation of Maughmer's winglets designed for the 15-meter Ventus 2.

3.2.2 PGEN Model

Two aircraft masses and respective CG locations were selected to model in PGEN, and are given in Table 3.1. The 330-kg case corresponds to a wing loading of 34 kg/m^2 (7 lb/ft^2), which is typical for flying in weak-moderate thermals. The 525 kg case corresponds to the sailplane maximum gross weight and supplies a wing loading of 54 kg/m^2 (11 lb/ft^2), which would be used for ridge flying or extremely strong thermal conditions. The cockpit loads and ballast amounts in both of these cases were selected to be achievable for flight testing in N597MD. The wing geometry used in PGEN closely models the planform of the Ventus 2bx, and is pictured in Figure 3.2. Seven wing panels are used to resolve the semi-span. The winglet itself uses three panels to capture its blending region, planform, and twist. The horizontal stabilizer is located and sized accordingly with the sailplane geometry. Fuselage flat plate area and pitching moment contributions are set from experience with similar configurations.

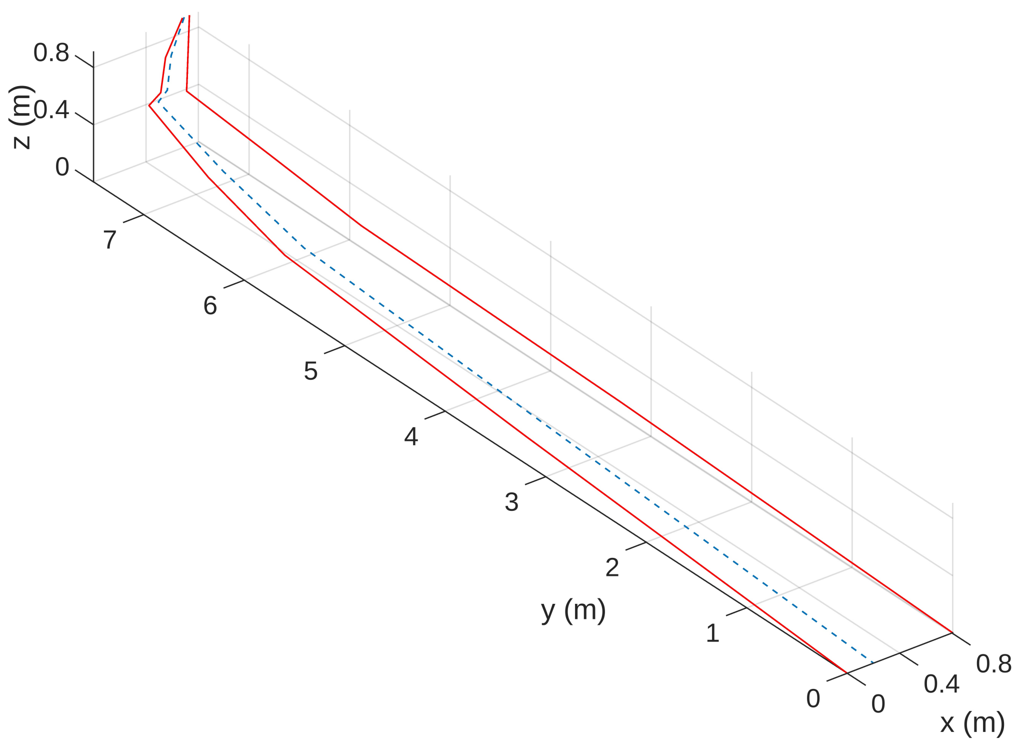

Figure 3.2. PGEN wing geometry for the Schempp-Hirth Ventus 2bx.

3.2.3 Winglet Geometry

The Ventus 2bx winglet geometry is presented in Figure 3.3. The two geometric panels resolving the winglet blade are shown with their respective inboard and outboard twist referenced to the body x-axis and the winglet airfoil zero-lift angle. The toe angle in this work is written as deviation from the fixed-geometry winglet root incidence, with positive toe defined to increase the winglet loading.

3.3 Methods

This thesis uses PGEN to create straight flight and turning polars for the Ventus 2bx with different flap settings and winglet toe angle positions. These polars are then collected and passed to simple MATLAB functions that search for and compile the optimum flap position/toe angle combination at every condition in both straight and circling flight. New straight-flight and circling polars are generated with these optimum

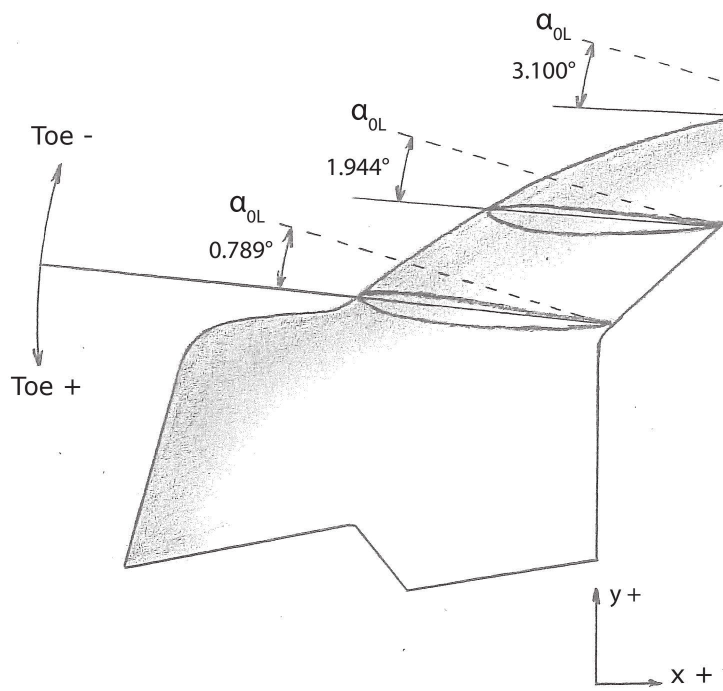

Figure 3.3. Ventus 2bx winglet geometry.

flap/toe combinations. The new polars are then used to predict the overall cross-country performance of the sailplane with variable-toe winglets. The sailplane was considered in both ballasted and unballasted configurations.

3.3.1 Assumptions and Constraints

The design approach used in this thesis applies the following constraints:

1. Existing winglet geometry is used (including twist distribution and planform shape) to permit flight test without constructing entirely new winglet blades.

2. It is assumed that varying the winglet toe angle does not measurably enhance the achievable C_L range of the variable-toe sailplane beyond what the unmodified sailplane is capable of.

3. The winglet toe angle varies less than 10° in total. Therefore, it is assumed that the winglet juncture remains cleanly sealed during flight and does not measurably increase the profile drag of the sailplane.

4. The flap positions of the stock sailplane were also used for the sailplane with variable-toe winglets.

5. The unballasted and ballasted CG locations were set with achievable cockpit loads for flight test.

6. Pilots do not necessarily use flaps L (20 degrees) for thermalling because it reduces aileron effectiveness and increases adverse yaw. When flaps L is used, it is usually exclusively for narrow and smooth thermals. Thus, the sailplane performance is assessed both with and without flaps L.

3.3.2 Polar Generating Workflow

Straight flight and turning polars were generated with PGEN for ranges of toe angles at each flap setting. This process was completed for both ballasted and unballasted cases using the workflow presented in Figure 3.4. PGEN's built-in flap optimization scheme was intentionally not used to avoid the unpredictable behavior it sometimes exhibits.

Straight flight and turning polars were created for the flap settings and toe angle ranges listed in table 3.2. These toe angle ranges for cruising and climbing flight were kept broad enough to definitively find the best-performing toe angle at every lift coefficient. Thus, initially predicting the ideal bounds of these ranges is less important than the ranges being wide enough to include the optimum toe angle; however, the toe angles selected reflect initial estimations as to what could be most beneficial throughout the flight envelope.

All polars were created using PGEN's total drag reduction scheme and were written for a speed range of 17–75 m/s. A total of 71 unballasted polars and 79 ballasted polars were analyzed. These polars were saved as individual text files and imported into MATLAB for further analysis.

3.3.3 Polar Optimization in MATLAB

Once all of the straight-flight and turning polars for the Ventus 2bx were generated and saved, they were imported into a MATLAB code to determine the combinations of characteristics that result in the highest-performing sailplane possible.

A simple optimization function was written to generate a straight flight polar with ideal flap/toe combinations. It searches for the highest performing flap/winglet configuration at every flight condition, and its structure is depicted in Figure 3.5. The resulting straight

Figure 3.4. Flow chart of polar-generating workflow. This approach was used for both of the sailplane weights modeled.

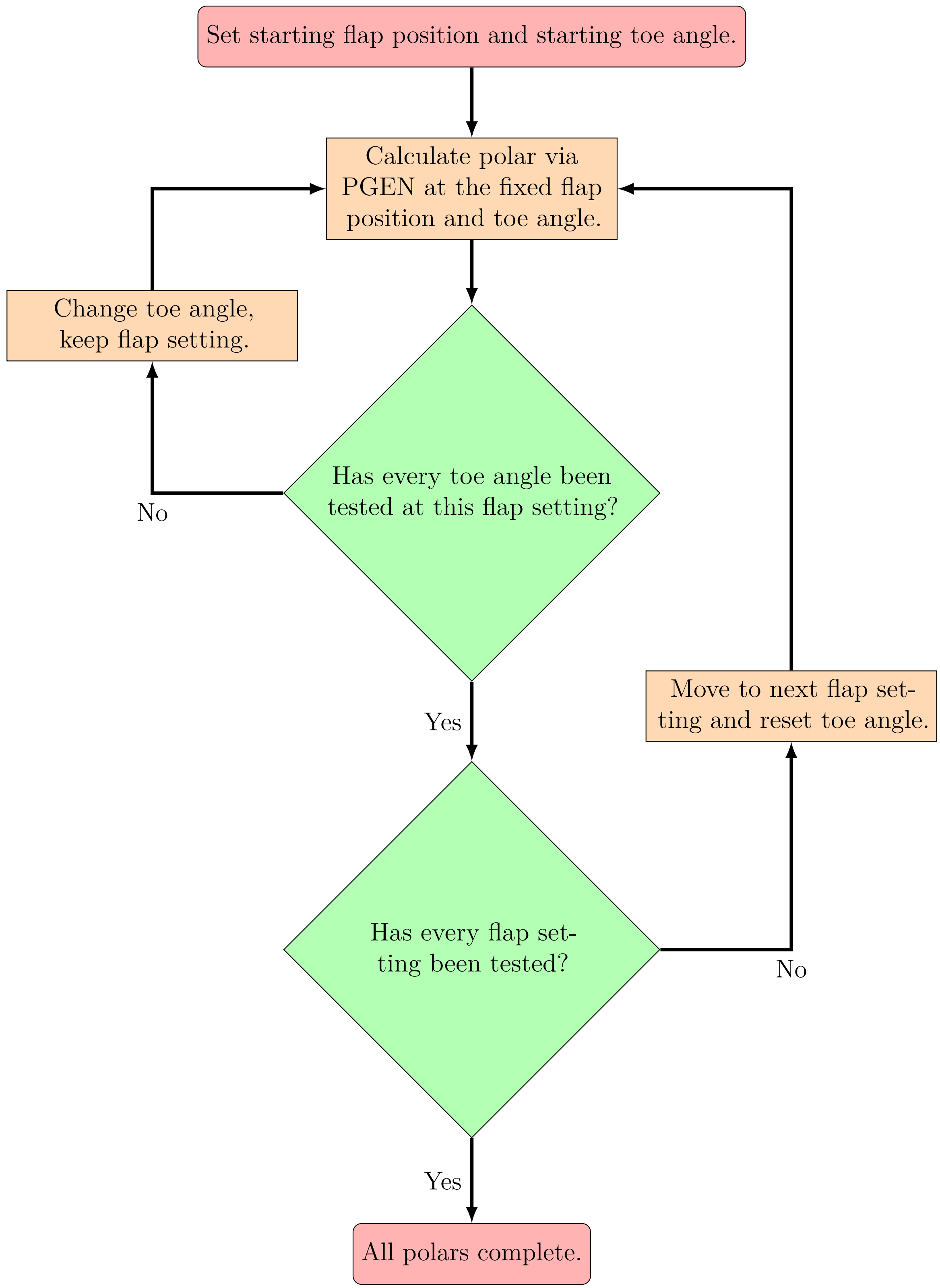

Figure 3.5. Structure of the optimization function written to generate the best-performing sailplane with variable-toe winglets.

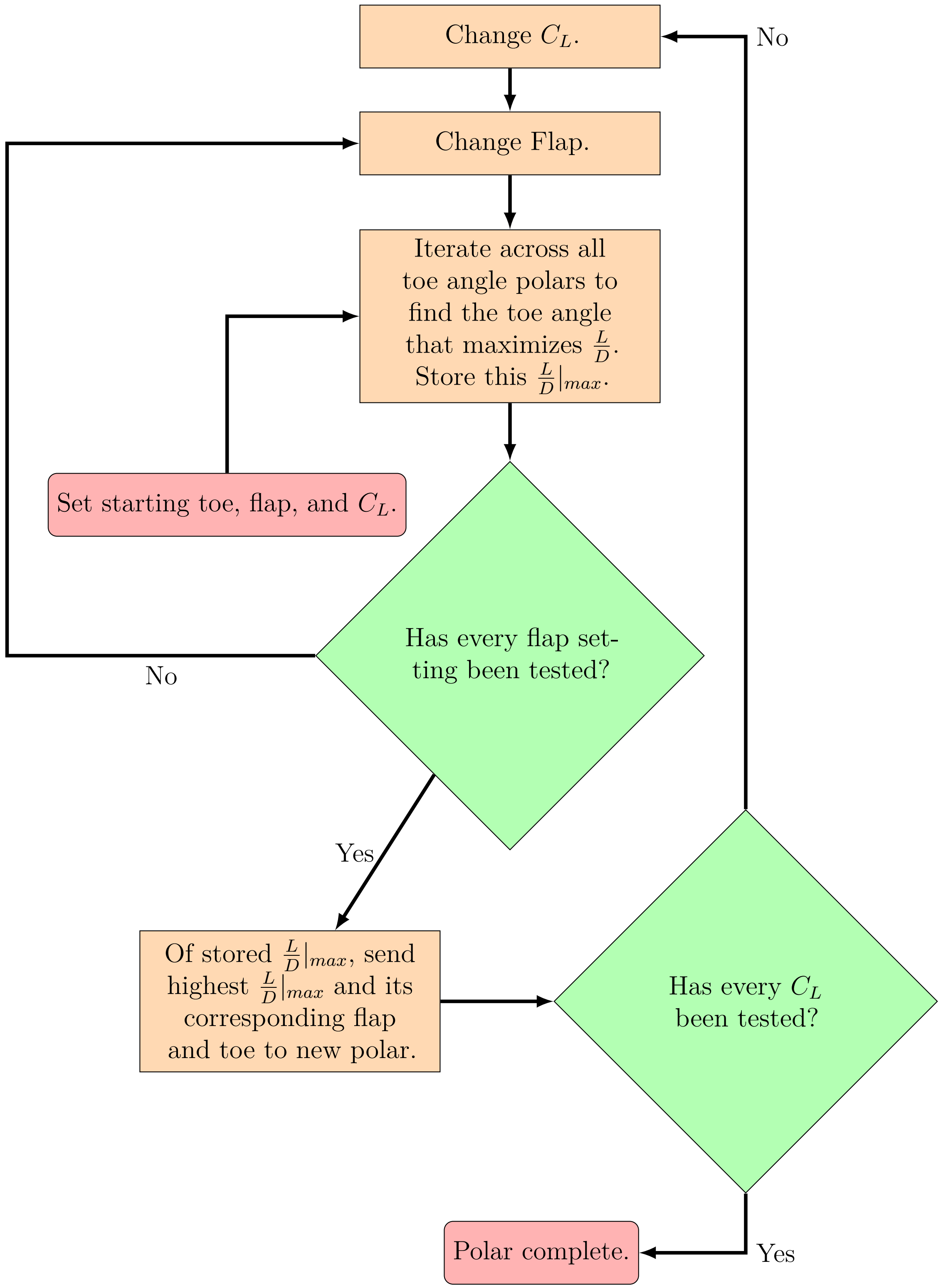

Flap Setting (Degrees Deflected)	330kg Toe Angle Range (0.5° Increments)	525kg Toe Angle Range (0.5° Increments)
S1 (−4.4°)	−2.0° → +0.5°	−2.0° → +1.0°
S (−1.9°)	−2.0° → +0.5°	−2.0° → +1.5°
–2 (0.0°)	−1.5° → +1.5°	−1.0° → +2.0°
–1 (+4.0°)	−0.5° → +2.0°	−0.5° → +3.5°
0 (+8.5°)	+0.0° → +2.5°	+0.0° → +4.0°
+1 (+13.5°)	+0.5° → +3.5°	+0.5° → +5.0°
+2 (+16.3°)	+1.0° → +5.5°	+0.0° → +5.5°
L (+20.0°)	+1.0° → +5.5°	+0.0° → +5.5°

Table 3.2. Toe angle ranges at each flap setting for which straight-flight and turning polars were generated. Polars were created for every toe angle at 0.5° increments within these ranges. Toe angles are written in degrees from the baseline toe angle.

flight polar was constructed from the flap/toe pairing that had the maximum L/D at each lift coefficient. In other words, this sailplane not only has a higher maximum L/D than the original Ventus 2bx, but it achieves a higher L/D at many flight conditions throughout its speed range. This is the true advantage of variable geometry.

Turning polars for the glider with variable winglets were generated in a similar way. The flap/toe combination that produced the lowest sink rate at each circling radius was selected.

These processes for generating straight flight and turning polars were repeated for four cases: 330kg including flaps L, 330kg excluding flaps L, 525kg including flaps L, and 525kg excluding flaps L.

Upon completion of polar generation in MATLAB, the final straight-flight and turning polars were saved as text files and used as input into the ACCS evaluator to compare the cross-country speeds of the variable-toe Ventus 2bx with the stock glider. Freewake was used to investigate individual flap/toe/C_L cases and compare the lift distributions and span efficiencies to the stock sailplane.

Chapter 4
Discussion of Results

4.1 Introduction

Overall, the modeling tools predict that variable-toe winglets meaningfully improve the performance of the Ventus 2bx within the context of modern sailplane design and competition soaring.

4.2 Toe-Angle Scheduling

The optimum predicted flap position and toe angle for every aircraft lift coefficient is plotted in Figure 4.1. The toe angle in this plot is represented as deflection from the baseline position; i.e., a toe angle of $0°$ corresponds to the toe angle used by the fixed winglets. Overall, these results are consistent with the broader understanding of the winglet operating regime. Larger toe angles are favored at low speeds/high lift coefficients–flight conditions in which increasing the winglet angle of attack further reduces spanwise flow and decreases induced drag. As the sailplane flies faster, the spanwise pressure gradients become weaker and the wing flowfield becomes more two-dimensional. Therefore, the importance of the winglet as an element that reduces spanwise flow is dimished at lower lift coefficients. Thus, the required winglet loading is reduced and the optimum toe angle decreases.

The lift coefficient at which the $0°$ toe angle occurs is analogous to the crossover point described by Maughmer and Kunz: the flight condition at which the winglet induced drag benefit is equal to its profile drag penalty. This is the singular place that the fixed winglets are optimum; any faster, and they hurt, any slower, and they help–but not as much as they could if the toe angle was increased. The location within the flight

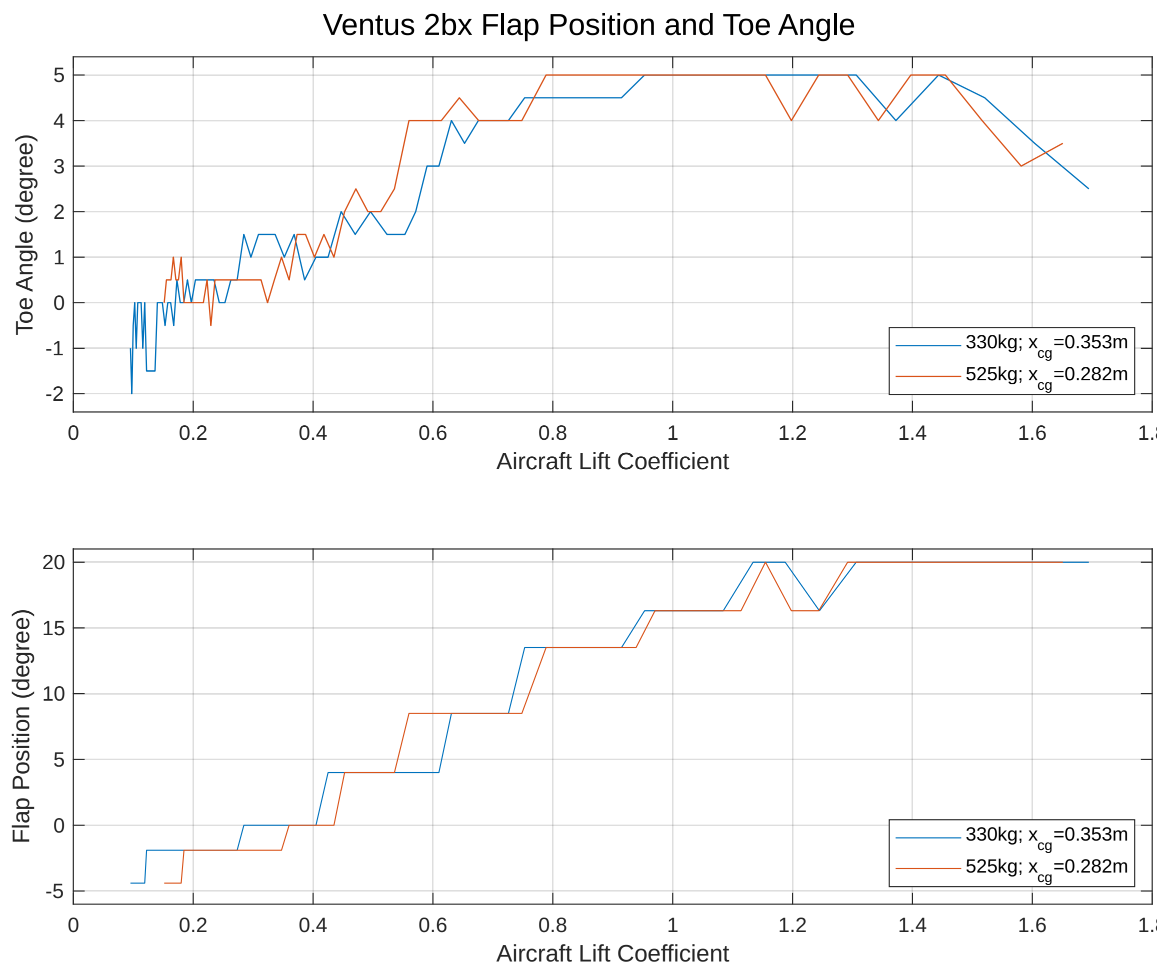

Figure 4.1. Optimum flap position and toe angle scheduled for the entire flight envelope of the Ventus 2bx. The toe angle is given in degrees from the baseline setting. Positive flap positions are trailing-edge down. The cases presented in this figure include flaps L.

envelope at which this 0° condition occurs represents how much climb performance the winglet designer has compromised to keep cruise performance acceptable. The Ventus 2bx winglets were not designed with the original crossover point method; however, sacrificing potential climb performance is the only way a designer can limit the cruising profile-drag penalties of fixed-geometry winglets. Thus, the crossover point of the fixed-geometry Ventus 2bx winglets is shifted to high enough speeds to be inaccessible for normal soaring flight. Consequently, the toe angles that maximize the sailplane L/D are different than the fixed winglet toe angle for nearly all of the sailplane flight envelope. This presents an excellent opportunity to improve the sailplane performance throughout its entire speed range.

The differences between ballasted and unballasted flap scheduling have two likely

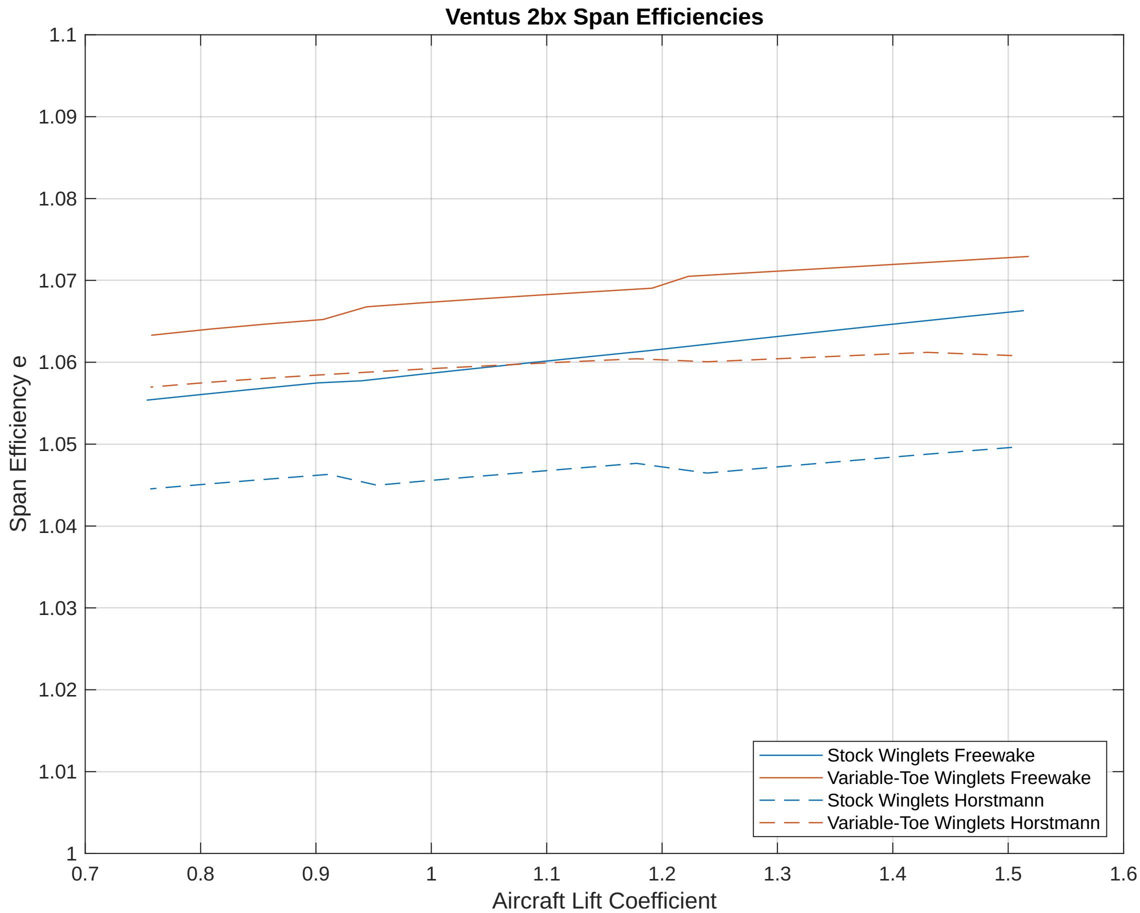

Figure 4.2. Comparison of predicted Freewake and Horstmann span efficiencies for the Ventus 2bx at climbing lift coefficients. This plot includes flaps L.

causes: the change in CG location between the two cases and the different Reynolds numbers encountered at every lift coefficient. The spikes in toe-angle scheduling are artifacts of PGEN's interpolation schemes and would be averaged when implemented onto the sailplane.

4.3 Comparison of Horstmann and Freewake

Figure 4.2 presents the span efficiencies predicted by Horstmann's method and Freewake for lift coefficients within the sailplane climbing envelope. Crucially, both codes project that the variable-toe winglets consistently achieve span efficiencies approximately 0.01 larger than the stock winglets, despite the differences between the Horstmann/Freewake results. The variations between the two codes are likely attributable to the influence of the wake rollup on the span efficiency, which is only resolved by Freewake. Given the

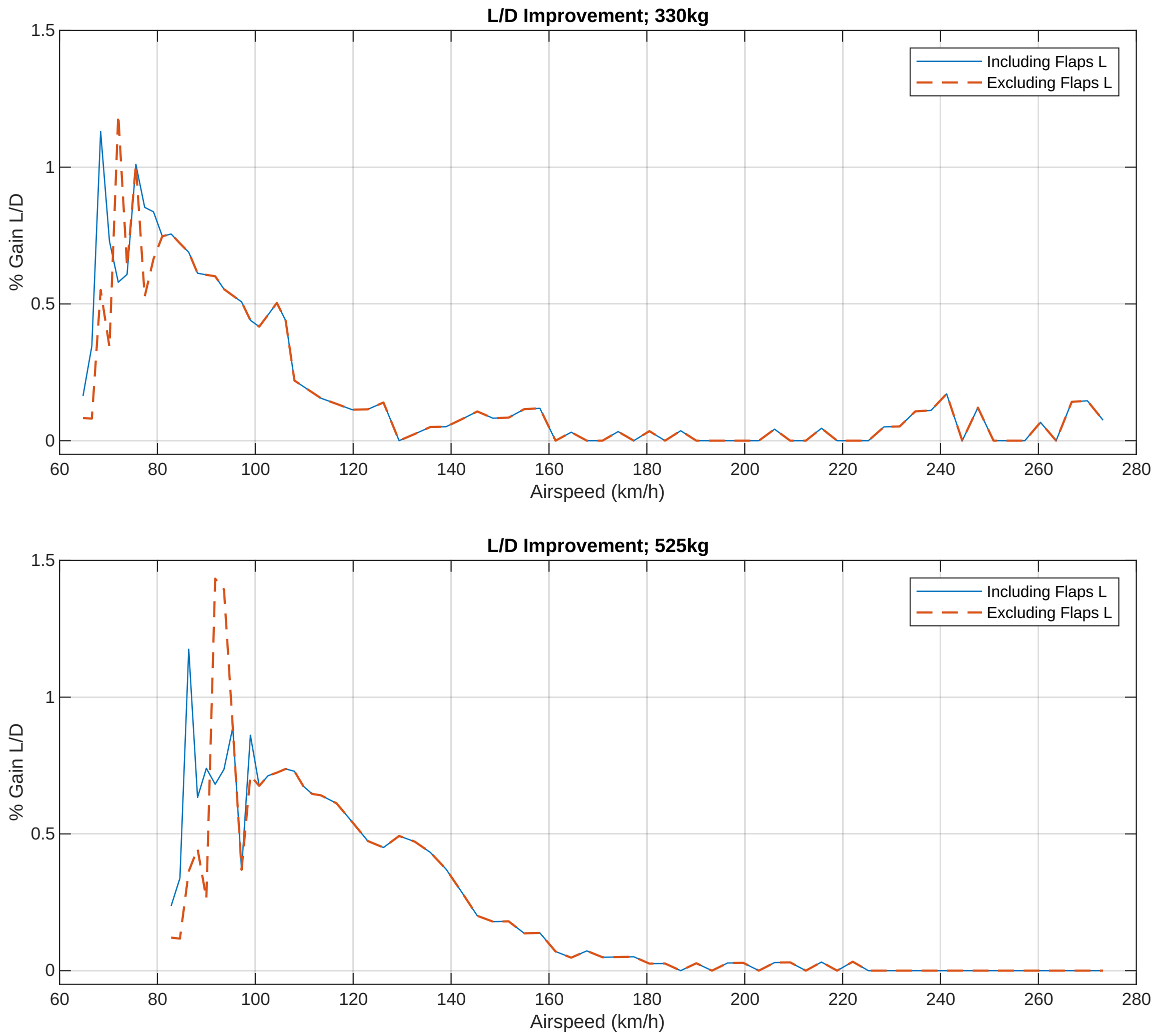

Figure 4.3. Improvements in the straight-flight performance of the Ventus 2bx with variable-toe winglets as a percentage of the baseline sailplane L/D.

consistency between both methods in predicting the improvements caused by variable-toe winglets, Freewake will be used when necessary to generate span lift distributions for individual cases. More comparisons between Freewake, Horstmann, and other singularity methods can be found in Refs. [4, 34, 35].

4.4 Straight-Flight Performance

The variable-toe winglets work as intended to access the performance that the fixed-geometry winglets compromise. As presented in Figure 4.3, the maximum gains are on the order of 1% of the baseline sailplane maximum L/D for both ballasted and unballasted cases. This corresponds to an approximate 0.5-point L/D improvement. As will be shown, these gains are substantial when applied to the entire operating regime of a high-performance sailplane. Additionally, these performance improvements are on the same order of those published in the literature reviewed in Chapter 1. As previously demonstrated in Figure 3.1, even small gains in L/D are within the capabilities of PGEN to assess.

4.4.1 Low Speed Cases

As shown in figures 4.1 and 4.3, the maximum performance benefits of variable-toe winglets occur at slow speeds. Larger toe angles have diminishing returns near the sailplane maximum lift coefficient. As the sailplane approaches stall, the Reynolds numbers on the winglet decrease to 150,000 or less. This substantially reduces local $c_{l_{max}}$ and increases $c_{d_{profile}}$. At these flight conditions, further raising the local angle of attack on the winglet increases its pressure drag and can even cause parts of it to stall prematurely. Separation measurably reduces the sailplane performance and inhibits handling qualities, despite the lesser importance of profile drag at low speeds. Consequently, the maximum winglet toe angle (baseline + 5°) is only optimum for a range of lift coefficients between 0.9 and 1.2. The optimum toe angle is reduced 2-3 degrees from the maximum value as the sailplane approaches stall. Toe angles greater than 5° were tested in PGEN but did not affect the sailplane performance as positively as the 5° cases.

4.4.2 High Speed Cases

The toe angle scheduling depicted in Figure 4.1 signals that the optimum winglet toe angle is a degree or two less than the baseline position at low lift coefficients. Winglets are not traditionally considered as devices that improve high-speed performance, so even small L/D improvements at this part of the flight envelope are results worth investigating. The mechanisms for these gains provide insight into the cruise design space for winglets, and could lead to larger performance advancements.

Figure 4.4 depicts the spanwise lift distributions of the Ventus 2bx in high-speed cruise with two different toe angles: the baseline setting, and the predicted ideal setting. The first consequential observation is that the local lift coefficients on the winglet at this flight condition are less than 0.13 for both cases, which is extremely low. Since the winglet airfoil laminar low-drag range ends at an approximate lift coefficient of 0.3, the profile-drag coefficient of the winglet increases substantially at these low lift coefficients.

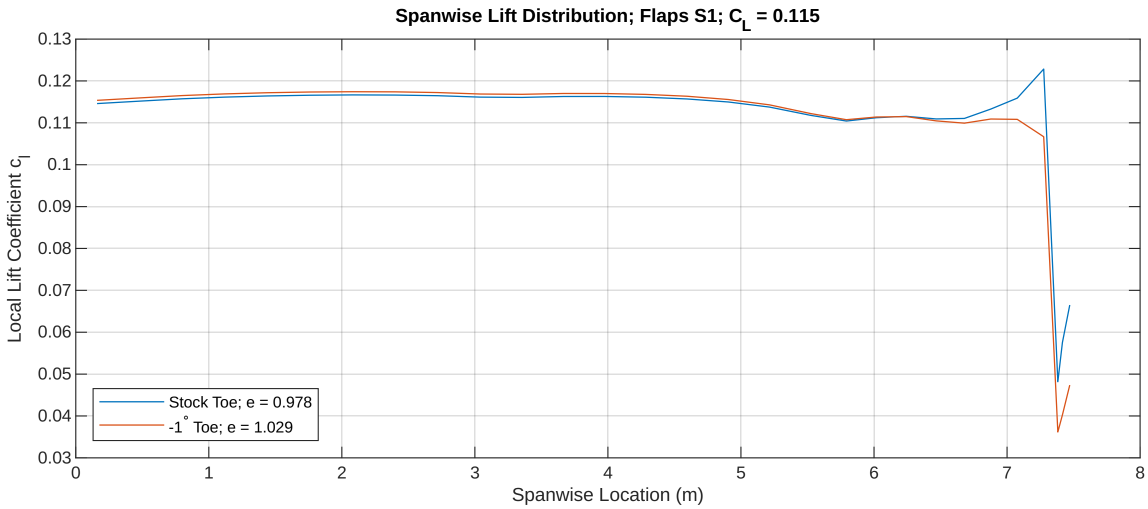

Figure 4.4. Freewake spanwise lift distributions of the stock Ventus 2bx and the variable-toe Ventus 2bx in high-speed cruise.

This issue is not limited to extreme conditions near the sailplane never-exceed speed. Since the wing/winglet are loaded at an approximately-uniform lift coefficient, the winglet reaches the bottom of its low drag range at sailplane lift coefficients as high as 0.3. This corresponds to a 95-knot, unballasted cruise speed and a 115-knot, which are commonly achieved during cross-country flights in average thermal conditions. Since the profile drag scales with V^2, keeping the winglet within its low drag range at higher speeds tangibly improves the sailplane performance. This will be discussed in Section 4.9.

The second insight provided by Figure 4.4 is that the baseline sailplane toe angle inefficiently over-loads the winglet and outboard wing in high-speed cruise. This presents the designer with a conundrum: the winglet airfoils are operating outside of their low drag range, but increasing the toe angle to raise the winglet lift coefficient is harmful to the span loading. The variable-toe winglets presented in this work cannot directly solve this problem; they can either improve the induced drag while further harming the profile drag, or vice versa. Interestingly, the more beneficial option in this case is the former. Reducing the toe angle 1° improves the sailplane span efficiency from 0.978 to 1.029 and measurably raises the L/D, even though this further impairs the winglet profile drag. This is a meaningful result because reducing induced drag is typically regarded as secondary to lowering the profile drag at high speeds. It also invites the question: can a winglet in cruise provide the optimum span loading while operating within the low-drag range of its airfoils, all without sacrificing climb performance?

The simplest answer to this question would entail designing a new winglet airfoil that achieves lower drag at smaller lift coefficients. Unfortunately, this would come at the cost of reducing the airfoil maximum lift coefficient, thereby compromising climb performance. This is a trade study worth pursuing, but will not be addressed further here. Since this work addresses variable geometry, another possibility is to place a flap on the winglet itself. Preliminary analysis for this promising concept will be presented later in this work.

4.5 Turning Performance

As described in Chapters 2 and 3, gains in straight-flight performance translate to improvements in circling performance. Accordingly, the Ventus 2bx configured with variable-toe winglets is superior to the unmodified glider in most turning cases. It is likely that some of these benefits are underpredicted by PGEN.

Figure 4.5 depicts the ballasted and unballasted optimum turning polars for the variable-toe Ventus 2bx and the unmodified glider. The most significant result presented by these plots is that variable-toe winglets improve the flaps +2 turning sink rates to be approximately equal to the flaps L turning sink rates in both ballasted and unballasted cases. If variable-toe winglets allow a sailplane to achieve flaps L circling performance in flaps +2, the pilot will be able to reliably access benefits that were only previously achievable under certain circumstances. As previously noted, thermalling in flaps L reduces aileron effectiveness, increases adverse yaw, and requires the pilot use more control deflection for the desired aircraft response. These are factors not considered by PGEN. Variable-toe winglets facilitate a sailplane to achieve flaps L circling performance without the attendant lateral-directional trim drag, while also permitting the pilot to more nimbly maneuver the sailplane to stay in the stronger parts of the updraft. These improvements are significant, and since they are not resolved by the analysis tools used, it is likely that these climbing benefits of variable-toe winglets are underpredicted. The variable-toe winglets most clearly benefit the sailplane circling performance for cases in which the sailplane is using flaps +2 rather than flaps L. Since the sailplane turning sink rate, as described in Equation (2.11), is related to $\frac{C_D}{C_L^{3/2}}$, it is initially tempting to attribute these gains to the variable-toe winglets permitting the sailplane to climb at a higher lift coefficient than the stock configuration. However, the opposite is true.

Since induced drag contributes most of the sailplane drag in climb, Equation (2.11) can be related to the induced drag coefficient defined in Equation (2.22) to compare

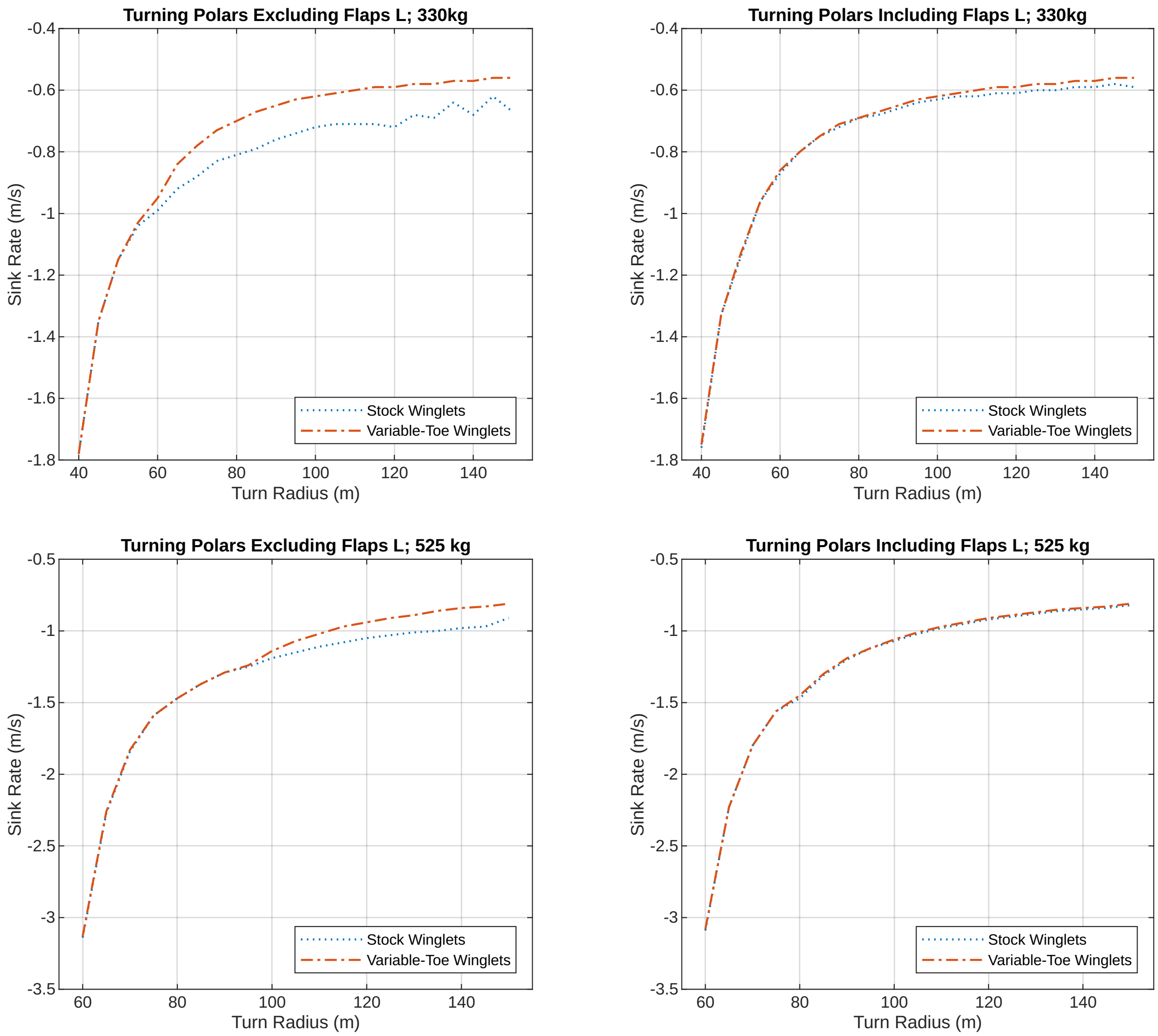

Figure 4.5. Turning polar comparisons for the Ventus 2bx with and without variable-toe winglets.

sailplanes having the same aspect ratio and wing loading at the same altitude:

$$V_{sink} \propto \frac{C_L^{1/2}}{e} \frac{1}{\cos^{3/2} \phi}. \tag{4.1}$$

To illustrate this point, Figure 4.6 shows the lift coefficients used to achieve the circling sink rates for the most beneficial case: 330kg without flaps L. As the turning radius increases, the minimum circling sink rate is achieved by flying slightly faster in a steeper bank. This technique decreases the aircraft induced drag by both lowering the lift coefficient and by operating the wing where the variable-toe winglets most improve the span efficiency. These coupled improvements are more substantial than the sink rate

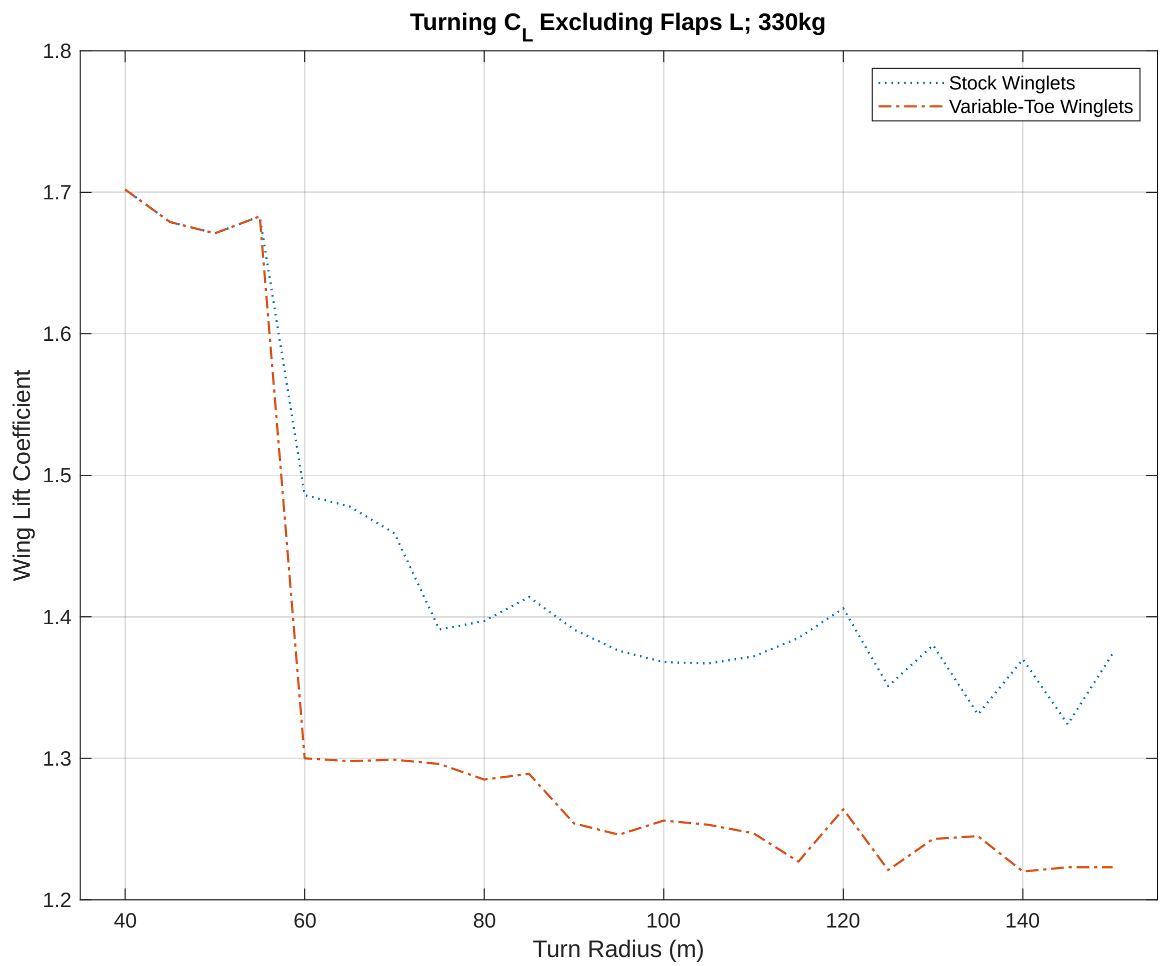

Figure 4.6. Wing lift coefficient used to achieve the minimum sink rate used at each turn radius.

penalty of flying at a slightly steeper bank angle. Figure 4.7 shows these differences in circling technique at an example turn radius of 120 meters: the sailplane with variable-toe winglets flies at a lift coefficient of 1.25 and a span efficiency of 1.07; the sailplane with stock winglets flies at a lift coefficient of 1.4 and a span efficiency of 1.06. Circling at a slightly lower lift coefficient also improves the thermalling stall margin.

4.6 Average Cross-Country Speed

It is important to consider the direct benefits of variable-toe winglets in climb and in cruise to understand their influence on the sailplane flight envelope; however, these improvements must be incorporated into the broader mission of a competition sailplane to define the tangible impacts of these performance improvements. As previously

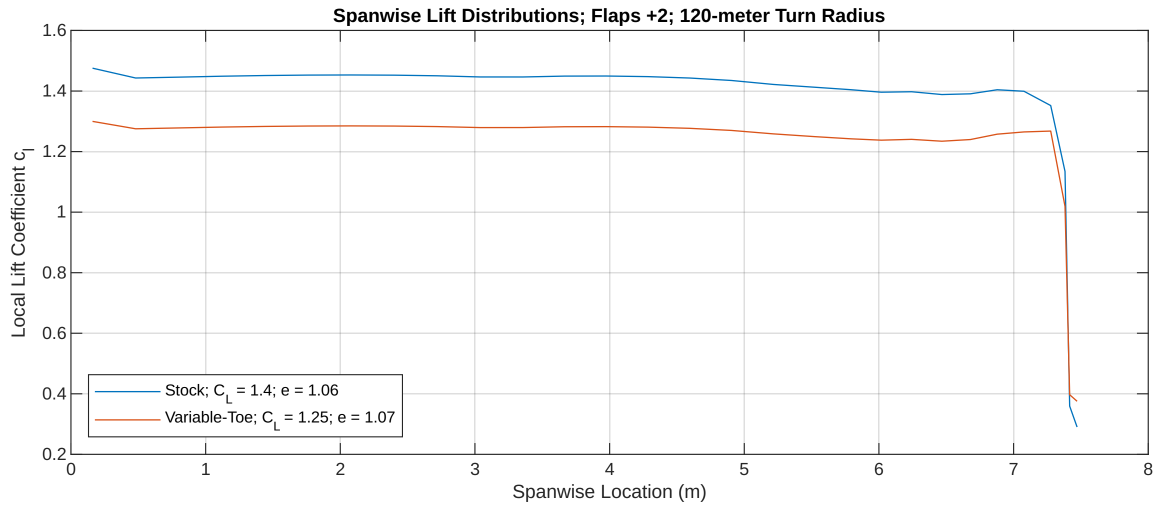

Figure 4.7. Freewake spanwise lift distributions for the Ventus 2bx with and without variable toe winglets at a circling radius of 120 meters.

established, MacCready cross-country speed is a consistent metric for evaluating sailplane cross-country performance. In this case, the climb and cruise benefits of the variable-toe winglets substantially improve the overall cross-country speeds of the Ventus 2bx, particularly in weak weather.

As derived in Chapter 2, the average cross-country speed of a sailplane flying in thermal conditions depends on three aspects of sailplane performance:

1. Maximizing the sailplane cruise speed between thermals.
2. Minimizing the sink rate endured by the sailplane at this cruise speed.
3. Maximizing the average climb rate achieved by the sailplane once it reaches the next thermal.

As previously described in this chapter, variable-toe winglets improve all three of these factors by positively affecting performance in cruise and in climb. This is the beauty of cumulative small gains: together, even modest improvements in straight-flight and turning performance act synergistically to meaningfully boost average cross-country speed.

Figure 4.8 depicts the gains in average cross-country speed achieved by the Ventus 2bx with variable-toe winglets, expressed as a percentage of the unmodfied sailplane average cross-country speed. The updraft velocity plotted is the maximum core strength of the thermals encountered. The achieved climb rate is substantially lower because the sailplane circles in these thermals at approximately 2/3 of the thermal radius, and the

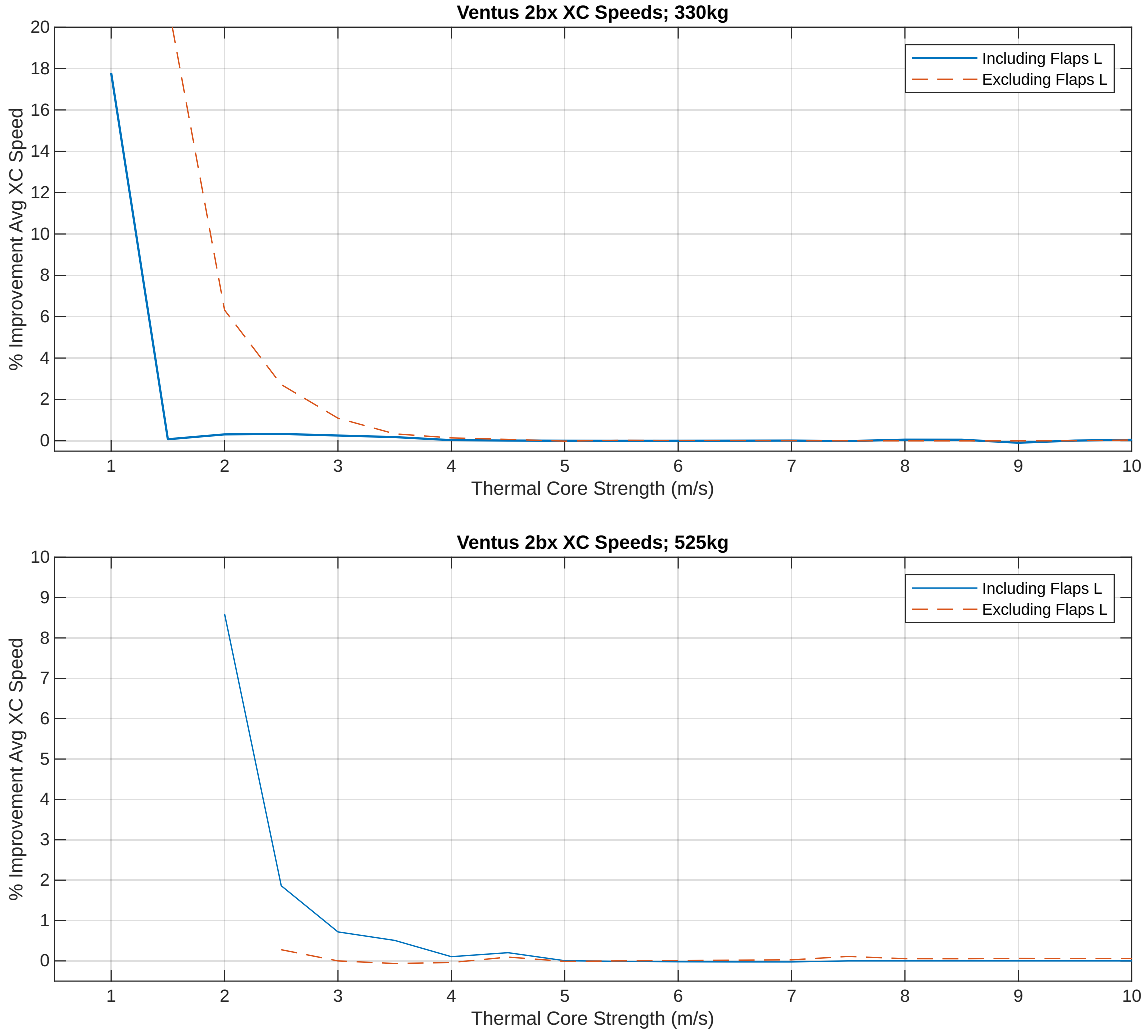

Figure 4.8. Improvements in the average cross-country speeds of the Ventus 2bx with variable-toe winglets as a percentage of the baseline sailplane L/D.

sailplane turning sink rate is superimposed on the thermal profile. It is clear that the greatest benefits of variable-toe winglets occur on days with weak thermals. Once again, this result is consistent with the purpose of this work: to unlock the climb benefits that fixed-geometry winglets compromise.

In weak weather, the sailplane flies entirely within the envelope that variable-toe winglets most benefit. The sailplane must use altitude sparingly in cruise because it takes longer to regain the height lost in weak updrafts. Thus, the wise pilot chooses a slower cruise speed to minimize the accompanying sink rate. At the lower end of the speed range, the variable-toe sailplane has the same straight-flight sink rate as the baseline sailplane at a meaningfully higher speed. Thus, the variable-toe sailplane flies faster between weak thermals with no additional penalty. Additionally, once the variable-toe sailplane reaches the next updraft, it will achieve a larger average climb rate than the unmodified sailplane because its circling sink rate is lower. This is especially significant in weak climbs, in which the sailplane sink rate is a substantial percentage of the updraft velocity.

The impressive gains in average cross-country speed presented in Figure 4.8 are consistent with these weak-weather benefits. In particular, the unballasted variable-toe Ventus 2bx has cross-country speeds on the order of 20% higher than the unmodified glider. For the flaps L case, this corresponds to average cross-country speeds about 1 km/hr faster than the stock glider on a day with 1.5 m/s thermals. The glider without flaps L is even more dramatic: it has average cross-country speeds a full 7 km/hr faster than the unmodified glider on a 1.5 m/s thermal day, and on a day with 1 m/s thermals, this glider can climb while the unmodified glider cannot. By itself, improving average cross-country speed as much as 1 km/hr can significantly improve the outcome of a contest day. Circumstances in which one sailplane can climb while the other must land are consequential to the outcome of the entire soaring contest.

The ballasted results are similar, although the magnitudes of the cross-country speed gains are smaller. This result is mostly caused by the turning polar improvement being less consistent for the ballasted cases. The average cross-country speed evaluation tool is sensitive to small differences in climb rate. Nonetheless, the maximum gains in cross-country speed are still on the order of 10%, which is very significant in the context of a soaring contest. Given the consistency of the other improvements predicted, the weaker results for the ballasted case excluding flaps L are regarded as an outlier.

As expected, the gains in cross-country speed diminish as the thermal strength grows because the sailplane increasingly operates outside of the portion of the flight envelope that the variable-toe winglets most improve. The differences between the modified and baseline sailplanes diminish at faster cruise speeds, and the climb rates in strong thermals are dominated by the updraft velocity rather than the sailplane turning polar.

The raw cross-country speeds for ballasted and unballasted cases studied are presented in Appendix B.

4.7 Contextualizing Gains

The gains in average cross-country speed presented in the preceding section signal that variable-toe winglets increase the effectiveness of the Ventus 2bx in the competition envi-

Day 1		Day 2		Day 3		Day 4		Day 5	
Speed (km/hr)	Points	Speed (km/hr)	Points	Speed (km/hr)	Points	Speed (km/hr)	Points	Speed (km/hr)	Points
128.88	1,000	112.97	1,000	112.32	1,000	147.55	979	110.58	1,000
128.78	998	112.94	1,000	112.05	996	147.13	974	110.18	993
128.50	994	112.79	997	112.00	995	145.27	951	109.49	983
128.47	994	111.05	966	111.23	982	*149.25*	*950*	109.36	980
128.20	990	111.03	966	110.55	971	144.68	943	109.25	979

Day 6		Day 7		Day 8		Day 9		Day 10	
Speed (km/hr)	Points	Speed (km/hr)	Points	Speed (km/hr)	Points	Speed (km/hr)	Points	Speed (km/hr)	Points
151.54	1,000	117.59	1,000	136.83	915	140.99	865	131.54	1,000
151.38	998	115.55	967	135.61	899	140.06	855	127.89	944
151.18	995	115.17	961	135.37	895	139.27	847	127.81	943
150.47	986	115.08	959	133.79	874	138.28	837	127.77	943
149.96	979	111.71	904	132.37	855	136.60	820	124.29	890

Table 4.1. Results for the 2023 15-meter World Gliding Championships in Narromine, Australia. The speeds and scores for the top five places are presented for every contest day. The fourth-place score on contest day 4 is the result of a start penalty.

ronment. To understand how significant these improvements are for possible competition results, scores from the 2023 15-meter World Gliding Championships are presented in Table 4.1.

On days 1, 2, 3, 5, and 6, the differences in achieved cross-country speed between the first-place pilot and the fifth-place pilot were less than 2 km/hr. These margins are well within the predicted improvements provided by variable-toe winglets. Of course, the achieved cross-country speed over a competition task is produced by factors not considered by MacCready, such as variation in thermal conditions throughout the task and cruising climbs in lift lines. The overall takeaway nonetheless applies: the competitive edge in a soaring contest can be achieved or lost by accumulation of mere seconds across a 500-kilometer task. These are precisely the kinds of gains that variable-toe winglets can reliably supply–particularly when compared with other modifications being implemented by sailplane manufacturers.

A compelling benefit of variable-toe winglets is that they can be designed with well-validated, classical methods. Horstmann's code and PGEN have been successfully utilized for the design and analysis of sailplane winglets since the late 1990s. These tools accurately predict the impact of different winglet geometries on the sailplane total drag and can be used rapidly in succession to assess the effects of design changes. While computational fluid dynamics (CFD) is a relevant and useful tool for evaluating specific aspects of a configuration that classical techniques cannot (such as juncture flows, fairings, and landing gear), it remains an inferior preliminary design tool because of its computational expense, run time, and the labor associated with generating grids and initiating a simulation.

Results from a CFD simulation of the Schempp-Hirth Ventus 3 from Ref. [6] are

C_L	Tailwheel + Fairing C_D	Pushrod Fairing C_D	ΔL/D	ΔL/D (%)
1.50	0.000047	0.000055	0.10	0.3
0.62	0.000048	0.000042	0.35	0.7
0.23	0.000049	0.000040	0.37	1.2

Table 4.2. Results from Ref. [6] presenting the CFD-predicted benefits of a retractable tailwheel and internal rudder drive for the Schempp-Hirth Ventus 3.

included in Table 4.2. These data show the impacts of adding a retractable tailwheel and eliminating the rudder control horn fuselage protrusions on the sailplane performance. These predicted gains are of the same order as those of variable-toe winglets, although they only meaningfully impact the sailplane at very high speeds. CFD studies such as this are important for advancing sailplane design, but these techniques are currently best suited for cases in which the geometry is well-defined and does not require significant optimization. It is likely that using CFD for preliminary design would be laborious with limited benefits. CFD could help the designer better understand the flow within the junctures of variable-toe winglets, but this step would be best once the concept is mature.

4.8 Build Methodologies and Considerations

The variable-toe winglets described in this work are intended to be implemented similarly to those prototyped by Weissenbuehler, Sullivan, and Maughmer for the Schempp-Hirth Nimbus 4. Installing variable-toe winglets on the Ventus 2bx is more challenging than the Nimbus because of the location of the Ventus water ballast tanks and the anatomy of the structural design; however, the following description is conceptually valid and these challenges could certainly be overcome. The additional weight to modify the Nimbus 4 was less than 10 pounds in total. This penalty is far outweighed by the performance benefits conferred by the variable-toe winglets.

4.8.1 Conceptual Design

Most basically, a hinge will be anchored into the sailplane wingtip that allows the winglet blade to change its toe angle, and the winglet itself will be actuated with a servo. Plywood ribs will transfer the winglet loads into the spar and skins of the main wing. The hinge point will be located as far inboard as possible, minimizing the width of the gap between the winglet and wing tip, while allowing the winglet to traverse the necessary range of

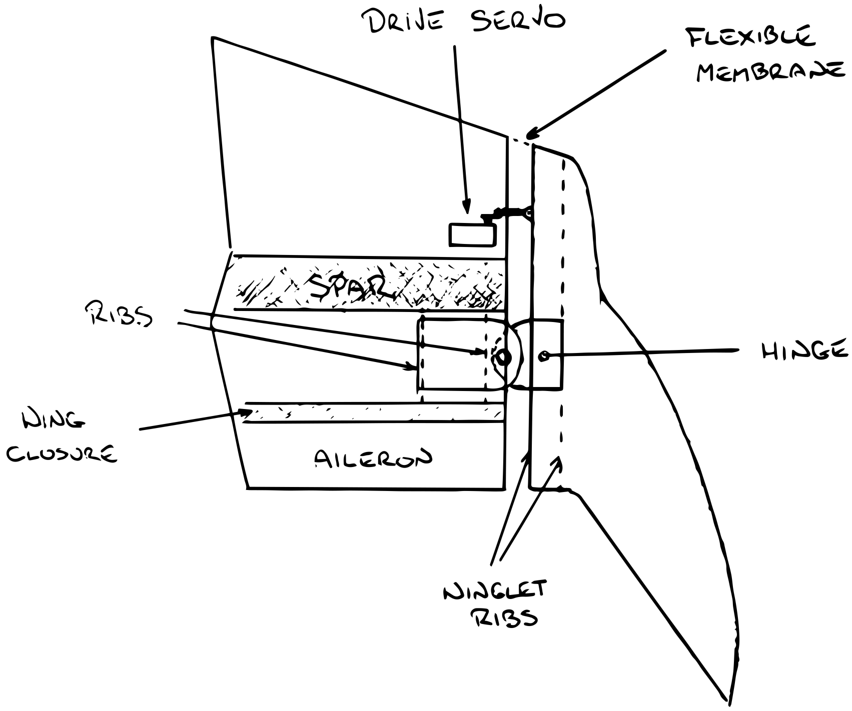

Figure 4.9. Variable-toe winglet conceptual sketch.

toe angles. The hinge will include mechanical stops at each end of the toe angle range. The winglet side of the hinge will slot into plywood ribs at the base of the winglet, and a pin will be used to secure the winglet blade onto the hinge and facilitate easy assembly. The hinge point will be located as close to the quarter-chord location of the winglet as possible. A servo will be located at the leading edge of the wing tip, and a rod will connect the servo to a fixture on the winglet root rib to actuate the winglet appropriately. A conceptual sketch of this is presented in Figure 4.9.

4.8.2 Control System

Initial versions of the variable-toe winglets described by this work could be actuated concurrently with the flaps via a flap position sensor. This would require establishing an average toe angle for each flap setting and relying on the pilot to correctly configure the sailplane at every flight condition. A future iteration of this concept could include flaps and winglets that automatically actuate together. This would include a flight computer that the pilot would use to set the wing loading for a specific flight, and an accelerometer to then determine the sailplane lift coefficient. The instantaneous aircraft C_L would then be filtered and used to specify the correct flap setting/toe angle. Automatic flap systems are currently flying successsfully on the Windward Performance Duckhawk, the experimental Nixus, and on some modified Schempp-Hirth Arcuses.

4.8.3 Structures and Certification

Most modern competition sailplanes are certified under the Experimental Exhibition/Air Racing category in the United States, which permits modifications without Supplemental Type Certificate or Field Approval. This greatly simplifies the effort associated with these types of alterations, reducing the required paperwork to an approval by an airframe technician during a condition inspection. Structurally, variable-toe winglets will not apply a significantly larger root bending moment than the fixed geometry winglets. The winglet loading is highest in climb, when the aircraft is below maneuvering speed. In cruise, the winglet loading is reduced as the toe angle decreases, and at the highest speeds the variable-toe winglets reduce the tip-loading below that of the fixed-geometry winglets.

4.9 Flapped Winglets

It has been shown that variable-toe winglets have potential to meaningfully advance the performance of a 15-meter competition sailplane by removing the low-speed compromises made by fixed-geometry winglets. However, even these significant improvements do not fully address the high-speed issues previously discussed. Therefore, the question has been raised: are there other ways to actuate a winglet that completely address its unique needs at both ends of the flight envelope?

Many sailplanes, including the Ventus 2bx, are designed with cruise flaps to broadly improve performance. These are somewhat unique to sailplanes, and serve two purposes. First, reflexing the airfoils on the wing decreases the pitching moment that the tail must resist, lessening the sailplane trim drag. Second, reducing the camber of the main wing shifts the location of the laminar low-drag range to lower lift coefficients, permitting the sailplane to achieve lower profile drag at higher speeds. Since the winglet operates outside of its low-drag range in cruise, incorporating a flap into the winglet is a possible way to reduce its profile drag while concurrently maintaining an ideal span loading. This is a meaningful advancement in design philosophy; conventionally, successful winglets make compromises to minimize harm in cruise. With a flap, the designer could actively

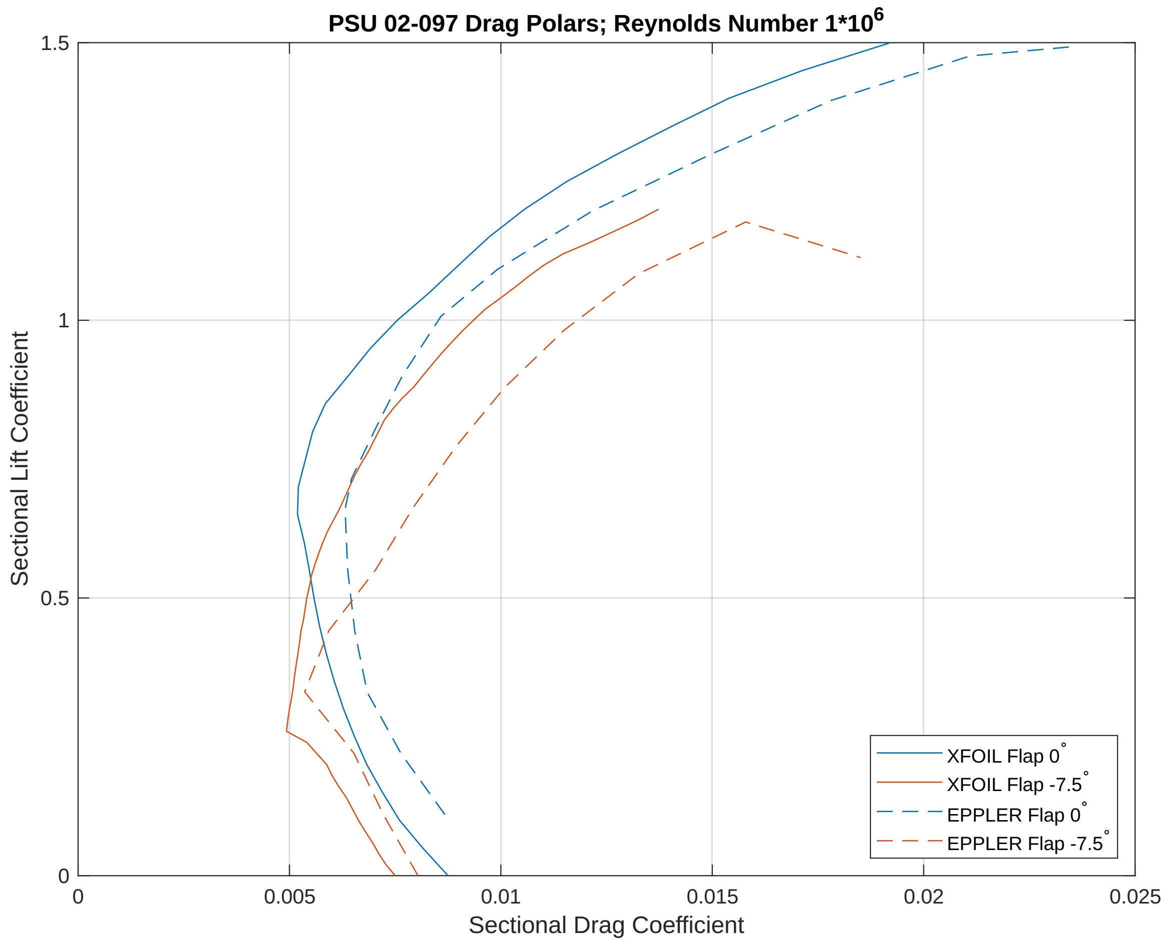

Figure 4.10. XFOIL and EPPLER polars for the PSU 02-097 winglet airfoil as implemented and with a 15% chord, −7.5° flap.

improve the sailplane cruise performance alongside with climb performance.

Figure 4.10 depicts XFOIL and EPPLER profile drag predictions of the Ventus 2bx winglet airfoil at a cruise Reynolds number of 1 million. The blue polars are for the winglet airfoil as installed on the baseline sailplane. The orange polars present the winglet airfoil with a 15% chord, −7.5° flap. With the flap deflected, both XFOIL and EPPLER shift the winglet low drag range to lower lift coefficients–reducing the profile drag by 15 counts at lift coefficients less than 0.5. These penalties occur at high enough speeds for even small increases in the profile-drag coefficient over the limited surface area of the winglet to measurably lower the entire sailplane L/D.

To test the validity of this concept, PGEN was used to predict the performance of the Ventus 2bx with a preliminary flapped winglet. XFOIL polars for the PSU 02-097 with a 15% chord flap were generated for +7.5°, 0°, and −7.5° deflections for Reynolds

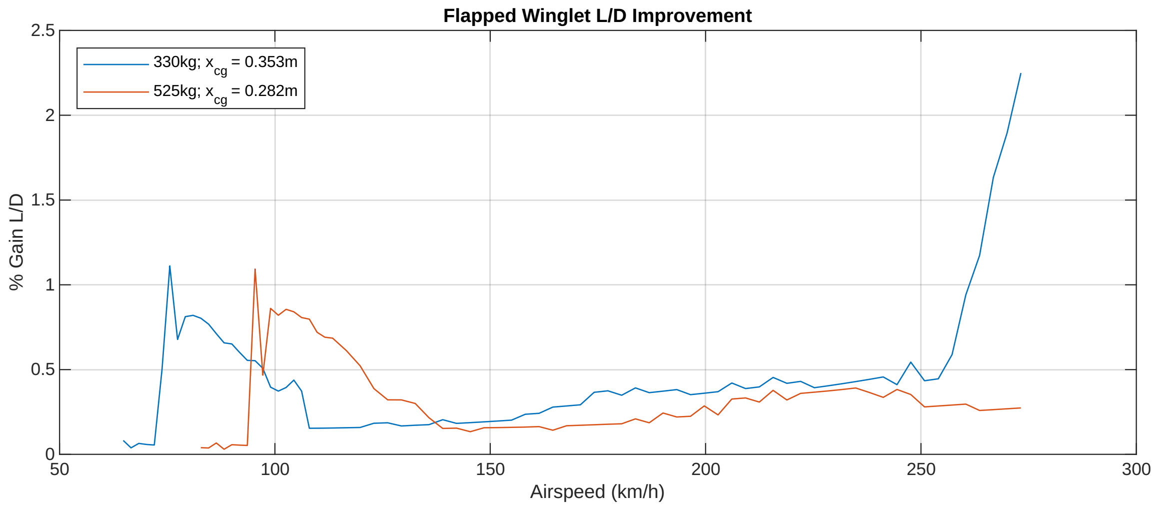

Figure 4.11. Improvements in the straight-flight performance of the Ventus 2bx with flapped winglets as a percentage of the baseline sailplane L/D.

numbers ranging from 35,000 to 1,600,000. The predicted values for $c_{l_{max}}$ were reduced by 0.2. The improvement in L/D of the sailplane with flapped winglets is expressed as a percentage of the baseline sailplane L/D in Figure 4.11.

The fundamental goal of this work is to improve sailplane cross-country speed by accessing previously-compromised induced-drag advantages of winglets. To stay true to this purpose, it is essential that flapped winglets offer the same climb advantages as the variable-toe winglets, and it is evident in Figure 4.11 that they do. The maximum L/D benefits for flapped winglets remains about 1% at low speeds–consistent with the previously shown improvements of variable-toe winglets in Figure 4.3. The exciting advantage of flapped winglets is that they outperform both the unmodified sailplane and the variable-toe sailplane substantially at high speeds, particularly at the low lift coefficients achieved when flying without ballast. Given that these results are for three, arbitrarily-selected flap deflections, it is conceivable that these gains could be even larger with some optimization effort. It has been shown that the accumulation of minor improvements can positively impact the outcomes of entire soaring contests. With flapped winglets, these small gains spread to larger portions of the flight envelope, and could even more meaningfully influence the sailplane operating environment.

The practical aspects of implementing flapped winglets onto a competition sailplane are also compelling when compared to variable-toe winglets. The actuator loads required to move a trailing-edge flap are less than for an entire winglet blade, and could be further reduced with a small aerodynamic balance. Flutter concerns could be directly addressed by mass-balancing the control surface, and the winglet juncture would remain cleanly sealed. The flap could be actuated with a torque tube connected to a gearbox or universal joint that link to a servo mounted in the sailplane wing tip, and this would require less structural modification of the sailplane wing.

Chapter 5 Conclusions and Future Work

5.1 Conclusions

Variable geometry is commonly leveraged to improve modern aircraft, with widely accepted examples including high-lift systems, constant-speed propellers, and variable stator vanes. These provide tangible advancements to the mature field of aircraft design. Likewise, sailplane design has reached a state in which achieving marginal gains requires extraordinary effort. The designer must decide which avenue provides the most meaningful boosts in performance with the fewest compromises elsewhere.

The overall goal of this work was to demonstrate that variable-toe winglets meaningfully improve the performance of a competition sailplane by avoiding the longstanding compromises of fixed-geometry winglets. The presented results are encouraging: variable-toe winglets permit the sailplane to fully realize the induced-drag benefits of winglets for climb. These low-speed improvements combine to substantially increase the achievable average cross-country speed of the Ventus 2bx in weak weather. The tools used to predict these gains are reliable and well-validated for sailplane winglet design, and in some cases underpredict the magnitudes of the performance gains. Variable-toe winglets are both competitive and appealing when considering the optimization difficulty of other modern sailplane performance enhancements.

A study that seeks to advance the state of the art must do so with as complete an understanding of the current state as possible. In this case, the work presented provides insight into the specific operating regime of sailplane winglets in cruise and guidance for better design. These are useful results for conventional and novel concepts alike.

5.2 Future Work

The performance benefits of any new aircraft system must be scrutinized along with the additional weight, complexity, and expense that it causes. These are operational factors not directly assessed in this work because they can only be truly understood from the experience accumulated over a season or two of contest flying. Unfortunately, a successful aircraft is not necessarily the highest-performing aircraft: it must also be reliable, pleasant to operate, and as inexpensive as possible. Excess performance is important, but it is not the only requirement. The previously-listed variable-geometry aircraft systems have earned their worth over years of successful implementation on many aircraft. Further work is necessary to better define the impacts of variable-geometry winglets on these fundamental operating constraints.

One of the other exciting results of this work is the potential for flapped winglets to even more broadly improve sailplane performance than variable-toe winglets. A concerted effort to optimize this concept could lead to improvements even larger than those presented here, and offer a promising solution to reliably enhance the performance of a competition sailplane.

The next step in advancing either of these concepts is construction and flight test. These efforts will include the specific design of the winglet actuation mechanism and control system. This work does not include flutter analysis, which is another worthwhile design step. Once the winglets are constructed, the best validation of their worth will be a season of contest flying. This is how fixed-geometry winglets earned the acceptance of competition pilots many years ago, and is the ultimate benchmark of the effectiveness of any sailplane modification.

Appendix A
Sailplane Polars

A.1 Variable-Toe Straight-Flight Polars

Polars for the Ventus 2bx with variable-toe winglets are published here. Baseline polars and polars excluding Flaps L are available on request, but will not be published here for brevity.

A.1.1 330kg Including Flaps L

V $(\frac{km}{hr})$	$C_{L_{wing}}$	C_L	C_D	V_{sink} $(\frac{m}{s})$	$\frac{L}{D}$	Flap (°)	Toe (°)
64.8	1.6699	1.6943	0.0692	0.74	24.47	20	2.5
66.6	1.5833	1.6039	0.0614	0.71	26.12	20	3.5
68.4	1.5035	1.5206	0.0486	0.61	31.32	20	4.5
70.2	1.4298	1.4436	0.0419	0.57	34.50	20	5
72	1.3614	1.3724	0.0376	0.55	36.45	20	4
73.8	1.2980	1.3062	0.0343	0.54	38.05	20	5
75.6	1.2328	1.2448	0.0311	0.53	39.99	16.3	5
77.4	1.1843	1.1876	0.0295	0.53	40.19	20	5
79.2	1.1331	1.1342	0.0277	0.54	40.97	20	5
81	1.0790	1.0843	0.0260	0.54	41.78	16.3	5
82.8	1.0343	1.0377	0.0243	0.54	42.66	16.3	5
84.6	0.9924	0.9940	0.0230	0.54	43.27	16.3	5
86.4	0.9531	0.9530	0.0217	0.55	43.85	16.3	5
88.2	0.9113	0.9145	0.0206	0.55	44.36	13.5	4.5
90	0.8766	0.8783	0.0196	0.56	44.80	13.5	4.5

91.8	0.8439	0.8442	0.0187	0.56	45.17	13.5	4.5
93.6	0.8131	0.8121	0.0179	0.57	45.36	13.5	4.5
95.4	0.7840	0.7817	0.0172	0.58	45.48	13.5	4.5
97.2	0.7565	0.7530	0.0165	0.59	45.55	13.5	4.5
99	0.7211	0.7259	0.0159	0.60	45.63	8.5	4
100.8	0.6965	0.7002	0.0153	0.61	45.76	8.5	4
102.6	0.6732	0.6758	0.0147	0.62	45.86	8.5	4
104.4	0.6510	0.6527	0.0142	0.63	45.89	8.5	3.5
106.2	0.6300	0.6308	0.0138	0.64	45.74	8.5	4
108	0.6005	0.6099	0.0134	0.66	45.58	4	3
109.8	0.5815	0.5901	0.0130	0.67	45.47	4	3
111.6	0.5634	0.5712	0.0126	0.68	45.31	4	2
113.4	0.5461	0.5532	0.0123	0.70	45.11	4	1.5
116.5959	0.5174	0.5233	0.0117	0.73	44.65	4	1.5
119.7918	0.4911	0.4958	0.0112	0.75	44.19	4	2
122.9878	0.4667	0.4703	0.0108	0.78	43.64	4	1.5
126.1837	0.4441	0.4468	0.0104	0.81	43.04	4	2
129.3796	0.4232	0.4250	0.0102	0.86	41.79	4	1
132.5755	0.3958	0.4048	0.0099	0.90	40.76	0	1
135.7714	0.3777	0.3859	0.0097	0.94	39.98	0	0.5
138.9673	0.3610	0.3684	0.0094	0.99	39.16	0	1.5
142.1633	0.3453	0.3520	0.0092	1.03	38.33	0	1
145.3592	0.3306	0.3367	0.0090	1.08	37.46	0	1.5
148.5551	0.3169	0.3224	0.0088	1.13	36.54	0	1.5
151.751	0.3040	0.3089	0.0087	1.18	35.62	0	1.5
154.9469	0.2919	0.2963	0.0085	1.24	34.72	0	1
158.1429	0.2806	0.2845	0.0084	1.30	33.85	0	1.5
161.3388	0.2664	0.2733	0.0083	1.36	33.05	-1.9	0.5
164.5347	0.2564	0.2628	0.0081	1.42	32.29	-1.9	0.5
167.7306	0.2468	0.2529	0.0080	1.48	31.53	-1.9	0
170.9265	0.2379	0.2435	0.0079	1.54	30.79	-1.9	0
174.1225	0.2294	0.2347	0.0078	1.61	30.06	-1.9	0.5
177.3184	0.2214	0.2263	0.0077	1.68	29.35	-1.9	0.5
180.5143	0.2138	0.2183	0.0076	1.75	28.68	-1.9	0.5
183.7102	0.2065	0.2108	0.0075	1.82	28.06	-1.9	0.5

186.9061	0.1997	0.2037	0.0074	1.89	27.49	-1.9	0.5
190.102	0.1932	0.1969	0.0073	1.97	26.83	-1.9	0
193.298	0.1870	0.1904	0.0073	2.05	26.18	-1.9	0.5
196.4939	0.1811	0.1843	0.0072	2.14	25.56	-1.9	0
199.6898	0.1755	0.1784	0.0072	2.22	24.95	-1.9	0
202.8857	0.1702	0.1728	0.0071	2.31	24.35	-1.9	0.5
206.0816	0.1650	0.1675	0.0070	2.41	23.77	-1.9	-0.5
209.2775	0.1602	0.1624	0.0070	2.51	23.19	-1.9	0
212.4735	0.1555	0.1576	0.0070	2.61	22.62	-1.9	0
215.6694	0.1511	0.1530	0.0069	2.72	22.05	-1.9	-0.5
218.8653	0.1468	0.1485	0.0069	2.83	21.48	-1.9	0
222.0612	0.1428	0.1443	0.0069	2.95	20.91	-1.9	0
225.2571	0.1389	0.1402	0.0069	3.08	20.35	-1.9	0
228.453	0.1350	0.1363	0.0069	3.21	19.79	-1.9	-1.5
231.649	0.1315	0.1326	0.0069	3.35	19.22	-1.9	-1.5
234.8449	0.1280	0.129	0.0069	3.50	18.66	-1.9	-1.5
238.0408	0.1247	0.1256	0.0069	3.65	18.10	-1.9	-1.5
241.2367	0.1216	0.1222	0.0070	3.82	17.55	-1.9	-1.5
244.4326	0.1141	0.1191	0.0070	3.99	17.03	-4.4	0
247.6286	0.1112	0.1160	0.0070	4.15	16.56	-4.4	-1
250.8245	0.1084	0.1131	0.0070	4.32	16.12	-4.4	0
254.0204	0.1057	0.1103	0.0070	4.49	15.71	-4.4	0
257.2163	0.1031	0.1075	0.0070	4.67	15.30	-4.4	0
260.4122	0.1005	0.1049	0.0070	4.86	14.89	-4.4	-1
263.6082	0.0981	0.1024	0.0071	5.05	14.49	-4.4	0
266.8041	0.0958	0.0999	0.0071	5.26	14.10	-4.4	-0.5
270	0.0935	0.0976	0.0071	5.46	13.73	-4.4	-2
273.1959	0.0913	0.0953	0.0071	5.69	13.35	-4.4	-1

A.1.2 525kg Including Flaps L

V ($\frac{km}{hr}$)	$C_{L_{wing}}$	C_L	C_D	V_{sink} ($\frac{m}{s}$)	$\frac{L}{D}$	Flap (°)	Toe (°)
82.8	1.6593	1.6509	0.0649	0.90	25.43	20	3.5
84.6	1.5914	1.5814	0.0593	0.88	26.69	20	3
86.4	1.5277	1.5162	0.0503	0.80	30.13	20	4

88.2	1.4679	1.4549	0.0436	0.73	33.37	20	5
90	1.4116	1.3973	0.0395	0.71	35.40	20	5
91.8	1.3585	1.3431	0.0364	0.69	36.93	20	4
93.6	1.3085	1.2919	0.0337	0.68	38.32	20	5
95.4	1.2550	1.2436	0.0313	0.67	39.70	16.3	5
97.2	1.2104	1.1980	0.0293	0.66	40.83	16.3	4
99	1.1746	1.1548	0.0282	0.67	41.01	20	5
100.8	1.1283	1.1139	0.0267	0.67	41.72	16.3	5
102.6	1.0904	1.0752	0.0254	0.67	42.39	16.3	5
104.4	1.0545	1.0384	0.0241	0.67	43.13	16.3	5
106.2	1.0204	1.0035	0.0230	0.68	43.7	16.3	5
108	0.9880	0.9704	0.0219	0.68	44.21	16.3	5
109.8	0.9522	0.9388	0.0210	0.68	44.75	13.5	5
111.6	0.9228	0.9088	0.0201	0.69	45.16	13.5	5
113.4	0.8948	0.8801	0.0193	0.69	45.52	13.5	5
116.5959	0.8484	0.8326	0.0181	0.70	46.04	13.5	5
119.7918	0.8055	0.7887	0.0171	0.72	46.22	13.5	5
122.9878	0.7566	0.7483	0.0160	0.73	46.63	8.5	4
126.1837	0.7200	0.7108	0.0152	0.75	46.85	8.5	4
129.3796	0.6862	0.6762	0.0144	0.77	46.93	8.5	4
132.5755	0.6547	0.6440	0.0137	0.79	46.85	8.5	4.5
135.7714	0.6255	0.6140	0.0132	0.81	46.47	8.5	4
138.9673	0.5982	0.5861	0.0128	0.84	45.96	8.5	4
142.1633	0.5727	0.5600	0.0123	0.87	45.37	8.5	4
145.3592	0.5394	0.5357	0.0119	0.90	44.97	4	2.5
148.5551	0.5171	0.5129	0.0115	0.92	44.70	4	2
151.751	0.4962	0.4915	0.0111	0.95	44.43	4	2
154.9469	0.4766	0.4714	0.0107	0.98	44.00	4	2.5
158.1429	0.4581	0.4526	0.0104	1.01	43.55	4	2
161.3388	0.4327	0.4348	0.0102	1.05	42.81	0	1
164.5347	0.4164	0.4181	0.0099	1.08	42.16	0	1.5
167.7306	0.4010	0.4023	0.0097	1.12	41.50	0	1
170.9265	0.3865	0.3874	0.0095	1.16	40.80	0	1.5
174.1225	0.3727	0.3733	0.0093	1.21	40.11	0	1.5
177.3184	0.3596	0.3600	0.0091	1.25	39.41	0	0.5

180.5143	0.3439	0.3473	0.0089	1.29	38.83	-1.9	1
183.7102	0.3322	0.3354	0.0088	1.34	38.22	-1.9	0.5
186.9061	0.3211	0.3240	0.0086	1.38	37.57	-1.9	0
190.102	0.3105	0.3132	0.0085	1.43	36.92	-1.9	0.5
193.298	0.3005	0.3029	0.0084	1.48	36.28	-1.9	0.5
196.4939	0.2909	0.2931	0.0082	1.53	35.64	-1.9	0.5
199.6898	0.2818	0.2838	0.0081	1.58	35.00	-1.9	0.5
202.8857	0.2732	0.2750	0.0080	1.64	34.36	-1.9	0.5
206.0816	0.2649	0.2665	0.0079	1.70	33.72	-1.9	0.5
209.2775	0.2570	0.2584	0.0078	1.76	33.07	-1.9	0.5
212.4735	0.2495	0.2507	0.0077	1.82	32.42	-1.9	0.5
215.6694	0.2423	0.2433	0.0077	1.88	31.80	-1.9	0.5
218.8653	0.2354	0.2363	0.0076	1.95	31.18	-1.9	0.5
222.0612	0.2288	0.2295	0.0075	2.02	30.59	-1.9	-0.5
225.2571	0.2225	0.2231	0.0074	2.09	29.99	-1.9	0.5
228.453	0.2164	0.2169	0.0074	2.16	29.40	-1.9	0
231.649	0.2106	0.2109	0.0073	2.24	28.77	-1.9	0
234.8449	0.2050	0.2052	0.0073	2.32	28.10	-1.9	0
238.0408	0.1997	0.1997	0.0073	2.41	27.41	-1.9	0
241.2367	0.1945	0.1945	0.0073	2.50	26.77	-1.9	0
244.4326	0.1896	0.1894	0.0073	2.60	26.13	-1.9	0
247.6286	0.1849	0.1846	0.0072	2.70	25.49	-1.9	0
250.8245	0.1758	0.1799	0.0072	2.79	25.00	-4.4	1
254.0204	0.1714	0.1754	0.0071	2.88	24.53	-4.4	0.5
257.2163	0.1672	0.1711	0.0071	2.97	24.07	-4.4	0.5
260.4122	0.1631	0.1669	0.0071	3.06	23.62	-4.4	1
263.6082	0.1592	0.1629	0.0070	3.16	23.18	-4.4	0.5
266.8041	0.1554	0.1590	0.0070	3.26	22.75	-4.4	0.5
270	0.1517	0.1553	0.0070	3.36	22.32	-4.4	0.5
273.1959	0.1482	0.1516	0.0069	3.46	21.91	-4.4	0

A.2 Variable-Toe Turning Polars

Turning polars for the Ventus 2bx with variable-toe winglets are published here. Baseline polars are available on request, but will not be published here for brevity.

A.2.1 330kg Including Flaps L

R (m)	V $(\frac{km}{hr})$	ϕ $(°)$	V_{sink} $(\frac{m}{s})$	$C_{L_{wing}}$	C_L
40	86.88	56.03	1.75	1.709	1.687
45	79.75	48.03	1.33	1.685	1.673
50	86.21	49.48	1.13	1.491	1.473
55	81.81	43.77	0.96	1.484	1.471
60	79.53	39.64	0.86	1.470	1.461
65	78.26	36.52	0.80	1.452	1.446
70	78.25	34.51	0.75	1.415	1.410
75	77.63	32.28	0.71	1.400	1.396
80	76.59	29.98	0.69	1.401	1.400
85	80.07	30.7	0.67	1.289	1.290
90	80.79	29.69	0.65	1.254	1.255
95	80.46	28.17	0.63	1.246	1.247
100	79.41	26.37	0.62	1.256	1.259
105	79.04	25.09	0.61	1.253	1.257
110	78.87	23.97	0.60	1.247	1.252
115	79.31	23.29	0.59	1.227	1.231
120	77.6	21.54	0.59	1.264	1.270
125	78.94	21.4	0.58	1.221	1.226
130	77.9	20.14	0.58	1.243	1.249
135	77.6	19.32	0.57	1.245	1.252
140	78.32	19.01	0.57	1.220	1.227
145	78.06	18.28	0.56	1.223	1.230
150	77.93	17.67	0.56	1.223	1.230

A.2.2 330kg Excluding Flaps L

R (m)	V $(\frac{km}{hr})$	ϕ $(°)$	V_{sink} $(\frac{m}{s})$	$C_{L_{wing}}$	C_L
40	86.88	56.03	1.78	1.702	1.687
45	79.75	48.03	1.35	1.679	1.673
50	75.69	42.02	1.15	1.671	1.672
55	72.62	37.02	1.03	1.683	1.690

60	89.57	46.4	0.95	1.300	1.287
65	86.12	41.89	0.84	1.298	1.289
70	83.61	38.17	0.78	1.299	1.294
75	82.06	35.21	0.73	1.296	1.293
80	81.32	33.05	0.70	1.285	1.283
85	80.07	30.7	0.67	1.289	1.290
90	80.79	29.69	0.65	1.254	1.255
95	80.46	28.17	0.63	1.246	1.247
100	79.41	26.37	0.62	1.256	1.259
105	79.04	25.09	0.61	1.253	1.257
110	78.87	23.97	0.60	1.247	1.252
115	79.31	23.29	0.59	1.227	1.231
120	77.60	21.54	0.59	1.264	1.270
125	78.94	21.4	0.58	1.221	1.226
130	77.90	20.14	0.58	1.243	1.249
135	77.60	19.32	0.57	1.245	1.252
140	78.32	19.01	0.57	1.220	1.227
145	78.06	18.28	0.56	1.223	1.230
150	77.93	17.67	0.56	1.223	1.230

A.2.3 525kg Including Flaps L

R (m)	V ($\frac{km}{hr}$)	ϕ ($°$)	V_{sink} ($\frac{m}{s}$)	$C_{L_{wing}}$	C_L
60	125.16	64.04	3.08	1.687	1.650
65	112.88	57.03	2.23	1.665	1.632
70	104.89	51.03	1.80	1.665	1.636
75	99.41	46.03	1.56	1.675	1.649
80	108.48	49.14	1.45	1.501	1.471
85	105.56	45.84	1.30	1.487	1.459
90	102.39	42.52	1.19	1.491	1.464
95	100.74	40.01	1.12	1.482	1.457
100	100.12	38.23	1.06	1.462	1.438
105	100.13	36.94	1.01	1.436	1.412
110	100.46	35.84	0.97	1.407	1.383
115	98.26	33.46	0.94	1.427	1.405

120	98.66	32.52	0.91	1.402	1.379
125	97.97	31.15	0.89	1.400	1.378
130	97.23	29.76	0.87	1.401	1.379
135	99.18	29.83	0.85	1.349	1.326
140	103.76	31.15	0.84	1.247	1.229
145	102.94	29.87	0.83	1.250	1.232
150	103.03	29.11	0.81	1.238	1.220

A.2.4 525kg Excluding Flaps L

$R\ (m)$	$V\ (\frac{km}{hr})$	$\phi\ (°)$	$V_{sink}\ (\frac{m}{s})$	$C_{L_{wing}}$	C_L
60	125.16	64.04	3.13	1.680	1.650
65	112.88	57.03	2.26	1.659	1.632
70	104.89	51.03	1.83	1.659	1.636
75	99.41	46.03	1.59	1.669	1.649
80	97.43	43.02	1.47	1.649	1.631
85	95.26	40.02	1.37	1.645	1.629
90	92.89	37.02	1.29	1.657	1.643
95	98.55	38.79	1.24	1.513	1.495
100	110.88	44.06	1.14	1.304	1.281
105	108.87	41.62	1.07	1.299	1.277
110	106.8	39.23	1.02	1.301	1.280
115	105.58	37.34	0.97	1.297	1.277
120	104.28	35.50	0.94	1.298	1.278
125	103.42	33.93	0.91	1.294	1.276
130	102.37	32.38	0.89	1.297	1.279
135	103.56	31.98	0.86	1.263	1.244
140	103.76	31.15	0.84	1.247	1.229
145	102.94	29.87	0.83	1.250	1.232
150	103.03	29.11	0.81	1.238	1.220

Appendix B
Cross-Country Speeds

B.1 330kg Cross-Country Speeds Excluding Flaps L

Variable-Toe Sailplane				Stock Sailplane			
Core ($\frac{m}{s}$)	V_{cruise} ($\frac{km}{hr}$)	V_{climb} ($\frac{m}{s}$)	V_{acc} ($\frac{km}{hr}$)	Core ($\frac{m}{s}$)	V_{cruise} ($\frac{km}{hr}$)	V_{climb} ($\frac{m}{s}$)	V_{acc} ($\frac{km}{hr}$)
1.0	105.514	0.021	3.378	1.0	none	none	none
1.5	121.384	0.397	41.528	1.5	120.752	0.300	34.272
2.0	134.394	0.791	62.086	2.0	124.137	0.705	58.394
2.5	143.747	1.192	76.306	2.5	143.272	1.127	74.287
3.0	152.856	1.597	87.281	3.0	152.600	1.557	86.338
3.5	171.353	2.005	96.676	3.5	171.267	1.990	96.352
4.0	186.572	2.432	105.179	4.0	186.527	2.425	105.033
4.5	192.098	2.866	112.708	4.5	192.102	2.861	112.633
5.0	200.754	3.303	119.430	5.0	200.761	3.304	119.450
5.5	202.996	3.747	125.505	5.5	203.006	3.744	125.473
6.0	211.602	4.187	130.894	6.0	211.556	4.186	130.876
6.5	213.725	4.629	135.882	6.5	213.727	4.628	135.874
7.0	219.011	5.072	140.485	7.0	218.971	5.072	140.484
7.5	221.069	5.517	144.700	7.5	221.094	5.517	144.704
8.0	223.144	5.963	148.571	8.0	223.085	5.964	148.577
8.5	228.301	6.41	152.221	8.5	228.283	6.411	152.230
9.0	230.299	6.858	155.641	9.0	230.281	6.859	155.650
9.5	232.382	7.326	158.965	9.5	232.398	7.326	158.965
10	236.986	7.776	162.016	10	234.367	7.776	161.954

B.2 330kg Cross-Country Speeds Including Flaps L

Variable-Toe Sailplane				Stock Sailplane			
Core ($\frac{m}{s}$)	V_{cruise} ($\frac{km}{hr}$)	V_{climb} ($\frac{m}{s}$)	V_{acc} ($\frac{km}{hr}$)	Core ($\frac{m}{s}$)	V_{cruise} ($\frac{km}{hr}$)	V_{climb} ($\frac{m}{s}$)	V_{acc} ($\frac{km}{hr}$)
1.0	105.573	0.040	6.289	1.0	101.964	0.034	5.339
1.5	124.785	0.423	43.387	1.5	121.796	0.424	43.355
2.0	126.414	0.825	63.662	2.0	134.648	0.825	63.466
2.5	150.484	1.242	77.842	2.5	150.397	1.233	77.585
3.0	153.280	1.660	88.735	3.0	153.227	1.650	88.510
3.5	171.819	2.082	98.259	3.5	171.740	2.073	98.084
4.0	187.007	2.511	106.640	4.0	186.977	2.509	106.607
4.5	192.493	2.939	113.877	4.5	192.509	2.938	113.864
5.0	201.118	3.369	120.389	5.0	201.117	3.369	120.386
5.5	203.275	3.801	126.190	5.5	203.270	3.801	126.190
6.0	211.833	4.234	131.451	6.0	211.811	4.234	131.449
6.5	213.884	4.669	136.312	6.5	213.917	4.669	136.305
7.0	219.133	5.107	140.823	7.0	219.164	5.105	140.809
7.5	221.162	5.540	144.911	7.5	221.152	5.543	144.932
8.0	223.170	5.982	148.728	8.0	223.145	5.972	148.648
8.5	228.373	6.426	152.347	8.5	228.329	6.416	152.269
9.0	230.397	6.872	155.746	9.0	230.451	6.892	155.894
9.5	232.434	7.345	159.093	9.5	232.476	7.343	159.078
10	237.002	7.795	162.140	10	234.463	7.793	162.062

B.3 525kg Cross-Country Speeds Excluding Flaps L

Variable-Toe Sailplane				Stock Sailplane			
Core ($\frac{m}{s}$)	V_{cruise} ($\frac{km}{hr}$)	V_{climb} ($\frac{m}{s}$)	V_{acc} ($\frac{km}{hr}$)	Core ($\frac{m}{s}$)	V_{cruise} ($\frac{km}{hr}$)	V_{climb} ($\frac{m}{s}$)	V_{acc} ($\frac{km}{hr}$)
2.5	136.345	0.328	39.105	2.5	139.566	0.328	38.997
3.0	157.839	0.677	63.458	3.0	157.839	0.677	63.458
3.5	179.391	1.051	81.052	3.5	179.398	1.052	81.104
4.0	187.799	1.418	94.751	4.0	187.834	1.420	94.789
4.5	199.340	1.788	106.026	4.5	196.177	1.789	105.926
5.0	214.082	2.161	115.363	5.0	214.090	2.161	115.376
5.5	215.828	2.535	123.834	5.5	215.806	2.535	123.833
6.0	227.132	2.911	131.174	6.0	227.152	2.911	131.160
6.5	228.850	3.290	137.912	6.5	228.844	3.288	137.887
7.0	233.708	3.670	143.909	7.0	233.744	3.668	143.871
7.5	235.431	4.062	149.473	7.5	235.382	4.049	149.308
8.0	240.284	4.446	154.416	8.0	240.245	4.439	154.331
8.5	241.914	4.831	158.973	8.5	241.880	4.823	158.888
9.0	273.145	5.217	164.260	9.0	273.144	5.209	164.157
9.5	273.144	5.605	168.916	9.5	273.143	5.596	168.815
10	273.167	5.994	173.205	10	273.164	5.984	173.106

B.4 525kg Cross-Country Speeds Inluding Flaps L

Variable-Toe Sailplane			
Core ($\frac{m}{s}$)	V_{cruise} ($\frac{km}{hr}$)	V_{climb} ($\frac{m}{s}$)	V_{acc} ($\frac{km}{hr}$)
2.0	134.558	0.091	13.741
2.5	149.713	0.411	45.903
3.0	164.661	0.740	66.880
3.5	179.536	1.076	82.117
4.0	187.967	1.446	95.662
4.5	199.489	1.817	106.818
5.0	214.169	2.190	116.086
5.5	215.950	2.565	124.459
6.0	227.313	2.942	131.755
6.5	228.977	3.321	138.426
7.0	233.889	3.702	144.376
7.5	235.565	4.092	149.875
8.0	240.416	4.476	154.787
8.5	242.065	4.861	159.311
9.0	273.150	5.247	164.635
9.5	273.147	5.635	169.260
10	273.150	6.024	173.520

Stock Sailplane			
Core ($\frac{m}{s}$)	V_{cruise} ($\frac{km}{hr}$)	V_{climb} ($\frac{m}{s}$)	V_{acc} ($\frac{km}{hr}$)
2.0	131.306	0.083	12.653
2.5	149.651	0.400	45.064
3.0	164.608	0.731	66.403
3.5	179.462	1.066	81.702
4.0	187.948	1.443	95.562
4.5	202.706	1.816	106.601
5.0	214.144	2.190	116.080
5.5	215.953	2.566	124.475
6.0	227.321	2.944	131.784
6.5	229.017	3.323	138.461
7.0	233.878	3.704	144.413
7.5	235.565	4.092	149.875
8.0	240.416	4.476	154.787
8.5	242.065	4.861	159.311
9.0	273.150	5.247	164.635
9.5	273.147	5.635	169.260
10	273.150	6.024	173.520

References

[1] Horstmann, K.-H., *Ein Mehrfach-Traglinienverfahren und seine Verwendung fur Entwurf und Nachrechnung nichtplanarer Flugelanordnungen*, Ph.D. thesis, Institut fur Entwurfsaerodynamik Braunschweig, 1987.

[2] Reichmann, H., *Cross-Country Soaring*, Thomson Publications, Santa Monica, CA, 1978.

[3] Thomas, F., *Fundamentals of Sailplane Design*, College Park Press, 1999.

[4] Bramesfeld, G., *A Higher Order Vortex-Lattice Method with a Force-Free Wake*, Ph.D. thesis, The Pennsylvania State University, 2006.

[5] Maughmer, M. D., "Design of Winglets for High-Performance Sailplanes," *Journal of Aircraft*, Vol. 40, No. 6, 2003, pp. 1099–1106.

[6] Axten, C. J., *Demonstrating the Potential of Transitional CFD for Sailplane Design*, Master's thesis, The Pennsylvania State University, 2019.

[7] Ohlmann, K., Federation Aeronautique Internationale Gliding Commision; Ratified, Current World Record: Free Distance up to 3 Turnpoints, Flight Date 21 Jan 2003.

[8] Lanchester, F. W., "Improvements in and relating to Aerial Machines," February 1898, British Patent No. 3608.

[9] Burnelli, V. J., "Airfoil Control Means," Uppercu-Burnelli Corporation, August 1930, US Patent No. 1774474.

[10] Mangler, W., "The Lift Distribution of Wings with End Plates," Tech. rep., National Advisory Committee for Aeronautics, April 1938, NACA Technical Memorandum No. 856.

[11] Hoerner, S. F., *Fluid-Dynamic Drag*, Hoerner Fluid Dynamics, 1965.

[12] Whitcomb, R. T., "A Design Approach and Selected Wind-Tunnel Results at High Subsonic Speeds for Wing-Tip Mounted Winglets," Tech. rep., NASA Langley Research Center, July 1976, NASA TN D-8260.

[13] McLean, D., "Wingtip Devices: What They Do and How They Do It," *Boeing Performance and Flight Operations Engineering Conference*, 2005.

[14] *FAA Supplemental Type Certificate ST00830SE*, Aviation Partners Boeing, Seattle, WA, September 2000.

[15] Dressler, U., "Aerodynamic Design of Winglets for a Standard-Class Glider," Vol. 17, OSTIV, 1983, pp. 42–50.

[16] Masak, P., "Winglet Design for Sailplanes," *Free Flight*, Vol. 2, 1992, pp. 6–8.

[17] Malinowski, M., *Aerodynamic Analysis of Morphing Geometry Application to Sailplane Winglet Design*, Master's thesis, Brno University of Technology, 2017.

[18] Guida, N. R., "Active Winglets," Tamarack Aerospace Group, Inc., March 2011, US Patent No. US007900877B1.

[19] *Tamarack Active Winglet System CJ Series Performance Planning Guide*, Tamarack Aerospace Group, Inc., 2020.

[20] Sankrithi, M. M. and Frommer, J. B., "Controllable Winglets," The Boeing Company, December 2008, US Patent No. US20080308683A1.

[21] Wildschek, A., Prananta, B., Kanakis, T., van Tongeren, H., and Huls, R., "Concurrent Optimization of a Feed-Forward Gust Loads Controller and Minimization of Wing Box Structural Mass on an Aircraft with Active Winglets," *16th AIAA/ISSMO Multidisciplinary Analysis and Optimization Conference*, Dallas, TX, June 2015.

[22] Dimino, I., Andreutti, G., Moens, F., Fonte, F., Pecora, R., and Concilio, A., "Integrated Design of a Morphing Winglet for Active Load Control and Alleviation of Turboprop Regional Aircraft," *Applied Sciences*, Vol. 11, No. 5, 2021.

[23] Cooper, J., Chekkal, I., Cheung, R., Wales, C., Allen, N., Lawson, S., Peace, A., Cook, R., Standen, P., Hancock, S., and Carossa, G., "Design of a Morphing Wingtip," *Journal of Aircraft*, Vol. 52, No. 5, 2015, pp. 1394–1403.

[24] Ursache, N. M., Melin, T., Isikveren, A. T., and Friswell, M. I., "Morphing Winglets for Aircraft Multi-phase Improvement," *7th AIAA Aviation Technology, Integration and Operations Conference*, Belfast, Northern Ireland, September 2007.

[25] Nagel, B., Kintscher, M., and Streit, T., "Active and Passive Structural Measures for Aeroelastic Winglet Design," *26th International Congress of the Aeronautical Sciences*, Anchorage, AK, 2008.

[26] Bourdin, P., Gatto, A., and Friswell, M. I., "Aircraft Control via Variable Cant-Angle Winglets," *Journal of Aircraft*, Vol. 45, No. 2, 2008, pp. 414–423.

[27] Falcão, L., Gomes, A. A., and Suleman, A., "Design and Analysis of an Adaptive Wingtip," *52nd AIAA/ASME/ASCE/AHS/ASC Structures, Structural Dynamics and Materials Conference*, Denver, CO, April 2011.

[28] Eguea, J. P., Catalano, F. M., Abdalla, A. M., de Santana, L., Venner, C. H., and Silva, A. L. F., "Study on a Camber Adaptive Winglet," *AIAA Aviation Forum*, Atlanta, GA, June 2018.

[29] MacCready, P. B., "Optimum Airspeed Selector," *Soaring*, Vol. 18, No. 2, 1954, pp. 8–9.

[30] Maughmer, M. D. and Kunz, P. J., "Sailplane Winglet Design," *Technical Soaring*, Vol. 22, No. 4, 1998, pp. 116–123.

[31] van Dam, C., "Natural Laminar Flow Airfoil Design Considerations for Winglets on Low-Speed Airplanes," Tech. rep., Vigyan Research Associates, Inc., 1984, NASA Contractor Report 3853.

[32] Maughmer, M. D., Swan, T. S., and Willits, S. M., "Design and Testing of a Winglet Airfoil for Low-Speed Aircraft," *Journal of Aircraft*, Vol. 39, No. 4, 2002, pp. 654–661.

[33] Kunz, P. J., *Development of a Software Package for the Assessment of High-Performance Sailplanes*, Master's thesis, The Pennsylvania State University, 1997.

[34] Coder, J. G., "Accuracy of high-order, discrete approximations to the lifting-line equation," *The Aeronautical Journal*, Vol. 127, No. 1315, 2023, pp. 1536–1553.

[35] Bramesfeld, G. and Maughmer, M., "Relaxed-Wake Vortex-Lattice Method Using DistributedVorticity Elements," *Journal of Aircraft*, Vol. 45, No. 2, 2008, pp. 560–568.

[36] Smith, S. and Kroo, I., "A Closer Look at the Induced Drag of Crescent-Shaped Wings," *AIAA 8th Applied Aerodynamics Conference*, Portland, OR, August 1990.

[37] Eppler, R., "Induced Drag and Winglets," *Technical Soaring*, Vol. 20, No. 3, 1996, pp. 89–96.